2

SUE: An ocean biogeochemical framework

2.1 Introduction

On time scales of decades and less the terrestrial biosphere exerts a significant control on atmospheric composition with a pronounced seasonal signal, primarily due to variability in the balance between uptake and release of CO_2 by the terrestrial biosphere [*IPCC*, 1990]. However, at some 39000 GtC the reservoir of dissolved carbon in the oceans is over 13 times that of the atmosphere and terrestrial biosphere put together [*IPCC*, 1994]. Thus, the mechanisms responsible for longer-term variability in the concentration of atmospheric CO_2 are more likely to involve the ocean. For this reason, models of the global carbon cycle used in the context of glacial-interglacial change are rooted in numerical representation of the oceanic carbon cycle.

Exchange of CO_2 between the ocean and atmosphere depends on the difference in molar fraction of gaseous CO_2 in the atmosphere (xCO_2) and in the surface ocean (assumed to be equal to its fugacity (fCO_2)). In the absence of any significant change in terrestrial ecosystem carbon storage, in weathering rates of silicate rocks, or in volcanic out-gassing of CO_2, it is the mean ocean surface fCO_2 (area-weighted and modified by local wind speed) that determines the value of xCO_2. fCO_2 in turn is primarily a function of the concentration of total dissolved inorganic carbon (DIC), alkalinity (ALK), salinity (S), and temperature (T) at the ocean surface. *Volk and Hoffert* [1985] recognized three main cycles of transformation of state and translocation within the ocean system which act to vertically (and horizontally) partition DIC and ALK and thus determine surface ocean fCO_2. These three processes were termed 'pumps', and comprise;

- The 'solubility pump', whose action arrises through the strong temperature-dependence of the solubility of gaseous CO_2 in water, with cold water exhibiting a much lower fCO_2 than warmer water. Thus, all other things being equal, warm oceanic regions will tend to be sources of CO_2 to the atmosphere and cold regions sinks. The concentration of atmospheric CO_2 is therefore related to mean sea surface temperature (SST).
- The 'soft tissue pump', whose effect is due to the removal of dissolved inorganic carbon from surface waters through its photosynthetic fixation by phytoplankton, and is subsequent export in the form of particulate organic carbon (POC) into deeper waters, where it is largely remineralized back into DIC. Through this action there is a vertical partitioning of DIC within the ocean with reduced surface concentrations. The concentration of atmospheric CO_2 is consequently inversely related to the strength of operation of this pump.
- The 'carbonate pump', whose effect arrises in a similar way to that of the soft tissue pump, except that the particulate phase in question is calcium carbonate ($CaCO_3$). In the production of $CaCO_3$ by certain species of phyto- and zoo-plankton and subsequent export, alkalinity is changed in a 2:1 ratio with DIC. The resultant alkalinity partitioning in the ocean more than counteracts the effect on fCO_2 of that due to DIC. The concentration of atmospheric CO_2 therefore scales with the strength of the operation of this pump.

At a minimum, any description of the global carbon cycle must resolve these three separate 'pumps'. However, the functioning of the real system is considerably more complicated than painted by this rather idealized picture. For instance, the soft tissue pump tends to 'leak', with a component of organic carbon primary production advected in a dissolved organic form as opposed to a pure vertical transport of particulates settling under the influence of gravity. The action of the soft tissue pump also results in a partitioning of alkalinity through the base capacities of the organic nutrients nitrate (NO_3^-) and phosphoric acid (PO_4^{3-}). This acts to slightly enhance the influence of the soft tissue pump on xCO_2. Regional variability in sea surface salinity (SSS) modifies the effect of the solubility pump, while regional differences in ocean surface wind speed and sea ice cover exert strong controls on the rate of gas transfer, thus influencing xCO_2. Finally, interactions between the ocean and underlying sediments plays an important role in influencing whole-ocean chemical and nutrient inventories on longer time scales.

Model structure is inevitably a trade-off between the degree of comprehensivity to which mechanisms within the global carbon cycle are represented, the spatial and temporal resolution of the model, simulation length, and actual model run-time. For a given requirement of simulation length together with practical and computational resource-driven limits on run-time, model structure is constrained by process complexity and spatial and temporal resolution. Additional constraints arise through deficiencies in our understanding of aspects of ocean biogeochemical cycling and in available data coverage and quality. Even so, there is no single solution in terms of a hypothetical 'optimal' model. Instead, model construction is inevitably a rather subjective 'art'.

2.2 Model description

For investigation of potential mechanisms driving the observed glacial-interglacial variability in xCO_2, a new numerical description of the (oceanic) global carbon cycle is developed in this study; a model named "SUE".

2.2.1 Framework overview

The model structure of SUE is shown schematically in Figure 2-1. SUE is essentially a biogeochemical framework of interactions important to the operation of the global carbon cycle operating on both an intra-ocean basis and across the interfaces linking atmosphere, ocean and deep-sea sediments. Ocean configuration and circulation are simply prescribed. As such, there is no feedback on the physical ocean from biogeochemistry and resulting atmospheric composition. Ocean-sediment interactions are described in Chapter 3. Typical model parameter values are summarized in Appendix IV. Full source code and example parameter files are attached on CD-ROM (Appendix V).

2.2.1.1 Ocean configuration and circulation

SUE is not tied to any particular ocean configuration but rather is developed as a flexible biogeochemical framework able to utilize any practical configuration of world ocean. In this, it is assumed that the ocean can be represented by a two-dimensional array of c horizontal regions or zones (hereafter referred to as 'grid points'), divided vertically into l vertical layers, giving a total of $c \times l$ distinct oceanic volumes ('cells'). To fully define the model physical ocean structure all that remains are the latitudinal and longitudinal boundaries (or alternatively the area) of each grid point region, together with the depth of the base of each ocean layer. Ocean circulation is defined by a set of mass flows between adjoining cells, from which the translocation of dissolved tracer species (such as DIC, ALK, and nutrients) can be calculated. Rather than prescribe entire ocean temperature (T) and salinity (S) fields as is usual in box model studies, temperature and salinity are advected along with other ocean tracers. Only SST and SSS boundary conditions must there be prescribed.

Many of the primary determinants of deep-sea sedimentary composition (such as $CaCO_3$ saturation state, and biogenic material rain rates) are depth-dependent. Assumption of a uniform depth for the ocean would then degrade the overall dynamics of ocean-sediment interaction [*Keir*, 1995]. In addition, the value of any comparison made between model sediments and observations will be reduced. The representation of deep sea sediments therefore follows previous schemes where the ocean floor is defined at each grid point according to a hypsographic curve [*Munhoven and Francois*, 1994, 1996; *Sundquist*, 1990; *Walker and Opdyke*, 1995], derived from actual (inferred) topography [*ETOPO5*, 1988] on either a mean regional or global basis. These continuous bathymetric profiles are discretized into a series of m separate depth bands at each grid point, with which an individual module handling ocean-sediment interactions is associated. The sediment module depth bands need not rigidly correspond to the depth intervals of ocean layers, with the result that changes in sea level can alter the depth in the ocean at which the sediments lie.

2.2.1.2 Overall biogeochemical cycling scheme

The model biogeochemical scheme is based around the cycling of three primary nutrients limiting to biological productivity; phosphate (PO_4), silicic acid (H_4SiO_4), and iron (Fe). Primary processes relating the intra-ocean cycling and ocean-sediment exchange of these nutrients in addition to dissolved inorganic carbon (DIC), alkalinity (ALK), and dissolved oxygen (O_2), are considered. Biogeochemical cycling is assumed to be representative of the 'open ocean' environment, with no explicit consideration of coastal or shelf processes (other than through highly parameterized representations of the accumulation and erosion of $CaCO_3$ and opal in neritic sediments – see 5.4.7). Carbon (as CO_2) and O_2 are exchanged with a 'well-mixed' atmosphere across the air-sea interface.

Nutrients, together with DIC and ALK, are taken out of solution in the sunlit surface ocean layer through biological action, and exported in particulate form (particulate organic matter (POM), $CaCO_3$, and opal) to deeper layers. As it settles through the water column, such material is subject to remineralization processes, resulting in the release of dissolved constituent species back to the ocean. Export of nutrients and carbon may also occur in the form of dissolved organic material (DOM). In this case, removal and transport is through ocean advection and mixing rather than gravitational settling. Dissolved iron in the ocean is considered in the form of a single species which is ultimately available for biological uptake at the ocean surface. In addition to surface biological removal dissolved Fe may also be taken out of solution throughout the ocean as a result of the scavenging action of settling particulate matter. Fe may therefore be subsequently released at depth back into solution not only through the normal operation of the 'soft tissue pump', but also liberated as the scavenging agents themselves are remineralized.

Biogenic and detrital material reaching the ocean floor may undergo diagenetic alteration (releasing further dissolved species to the ocean) and/or (semi-) permanent burial. The dissolution flux and thus fractional preservation of $CaCO_3$ and opal is represented mechanistically (Chapter 3). As an initial approximation, POM is preserved in a simple fraction, while Fe (whether in organic or inorganic form) reaching the sediments is assumed to be completely preserved along with detrital matter. Loss of material through burial in the sediments must be balanced over the long-term by supply to the ocean from continental weathering and geothermal processes (in the case of DIC, ALK, PO_4, and H_4SiO_4) together with aeolian input at the surface (Fe and H_4SiO_4).

The two stable isotopes of carbon (^{12}C and ^{13}C) are treated separately, with all significant fractionation processes involving transformations of carbon state taken into account. However, many of the most important fractionation processes discriminating between the stable isotopes of oxygen (^{16}O, ^{17}O, and ^{18}O) are associated with the operation

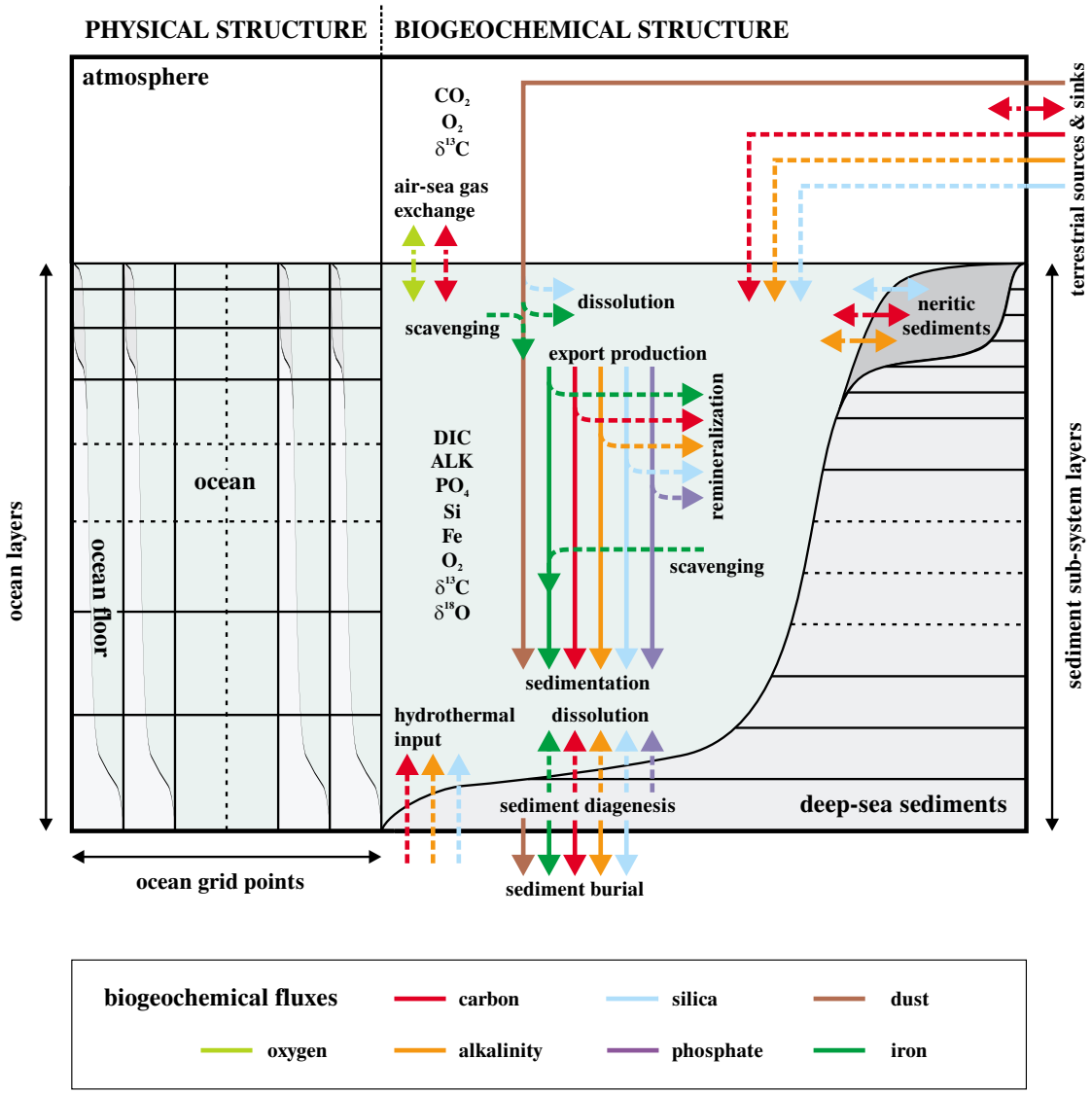

Figure 2-1. Schematic representation of the global carbon cycle model "SUE". Solid biogeochemical fluxes are shown as solid lines, dissolved fluxes are dashed lines, and gaseous fluxes as dotted lines.

of the hydrological cycle and terrestrial ecosystems, neither of which are explicitly represented in SUE. ^{18}O is therefore included only as a passive tracer. As such, it takes a (uniform) value throughout the ocean-atmosphere system set according to SPECMAP [*Imbrie et al.*, 1984] for any point in time.

2.2.1.3 Carbonate system thermodynamics

In order to calculate important variables such as the fugacity of CO_2 in the surface ocean, or the degree of under-saturation of $CaCO_3$ in the deep sea, the equilibrium state of the aqueous carbonate system must be known. A solution for this is approximated numerically given the concentrations of DIC, ALK, H_4SiO_4, and PO_4^{3-}, together with ambient temperature, salinity, and pressure. The thermodynamical scheme is outlined in Appendix I.

2.2.1.4 Numerical scheme

The incarnation of SUE presented here is rooted in mean annual ocean circulation in common with many other carbon cycle models. Equations describing intra-ocean and ocean-atmosphere processes are solved numerically within a forward-time finite difference framework. However, while this and similar schemes are numerically stable for ocean models having a relatively thick (≥150 m) surface ocean layer (e.g., *Broecker and Peng* [1986], *Keir* [1988]), instabilities in the air-sea exchange of CO_2 can arise if a much thinner surface ocean layer is assumed. The time step for intra-ocean and ocean-atmosphere processes is therefore allowed to take a value much shorter than 1 year. Problems can also arise with regards to the description of biological new production in the surface ocean, where there can be a danger of nutrient depletion below zero occurring [*Sarmiento et al.*, 1993]. A separate sub-step is therefore used for this, nested within that for the ocean-atmosphere system as a whole. Deep-sea sedimentary processes are solved strictly at an annual time step, and are asynchronously coupled with the ocean across the sediment-ocean interface at this same period.

2.2.2 Ocean-atmosphere gas exchange

In addition to being linked through ocean transport, surface ocean cells are geochemically coupled via the atmosphere. A single 'well-mixed' box is assumed on the basis of the relatively rapid rate of atmospheric mixing between the hemispheres compared with typical time scale of CO_2 concentration adjustment to changes in sources and sinks [*IPCC*, 1990]. Exchange of $^{12}CO_2$, $^{13}CO_2$, and O_2 between atmosphere and ocean across the air-sea interface is considered.

2.2.2.1 Ocean-atmosphere CO_2 exchange

Carbon cycle models have often used a prescribed gas transfer coefficient, taken to be uniform over the entire ocean surface [*Heinze et al.*, 1991, 1999; *Maier-Reimer*, 1993; *Maier-Reimer and Hasselmann*, 1987; *Marchal et al.*, 1998b; *Yamanaka and Tajika*, 1996]. The value assumed for this coefficient (typically between 0.05 and 0.07 mol m^{-2} μatm^{-1} a^{-1}) is taken consistent with ^{14}C observations [*Broecker et al.*, 1985]. Although wind speeds actually exhibit substantial spatial heterogeneity [*Broecker et al.*, 1985], on the basis that the effect of sea ice cover at high latitude regions would act so as to largely cancel out the influence of the higher wind speeds found there *Siegenthaler and Joos* [1992] supported the use of this uniform coefficient. However, on glacial-interglacial time scales both wind speed and sea ice extent are likely to vary significantly and independently of each other. It has been suggested that changes in either or both of these ocean surface boundary conditions may account for much of the observed atmospheric CO_2 record [*Keir*, 1993; *Stephens and Keeling*, 2000]. For this reason the influence of wind speed and sea ice extent on the mean gas transfer coefficient is taken into account at each grid point. The gas transfer coefficient is represented as an explicit function of wind speed in a similar manner to *Aumont et al.* [1999], utilizing an empirical description of gas exchange coefficient [*Wanninkhof*, 1992]. This relationship is then corrected for the application of long-term mean rather than instantaneous wind speeds [*Wanninkhof*, 1992]. In this, the flux density across the air-sea interface of each cell is

$$f_{\mathrm{atm}\rightarrow\mathrm{ocn}}^{\mathrm{CO_2}} = K \cdot \left(p\mathrm{CO}_2 - f\mathrm{CO}_2 \right) \tag{2-1}$$

where $p\mathrm{CO}_2$ is the partial pressure of CO_2 in the atmosphere, taken to be equal to its molar fraction ($x\mathrm{CO}_2$) for a mean atmospheric pressure of 1 atm, and $f\mathrm{CO}_2$ is the fugacity of CO_2 in the surface ocean. K is a gas transfer coefficient, expressed

$$K = k_{\mathrm{av}} \cdot Q \tag{2-2}$$

where k_{av} is the gas transfer velocity or piston velocity for appropriate for long-term average wind speeds (in m s^{-1}), and Q is the Henry's Law constant for CO_2 in seawater (calculated from *Weiss* [1974], and converted into units of mol m^{-3} μatm^{-1}). k_{av} is given by

$$k_{\mathrm{av}} = l \cdot \left[2.5 \cdot (a + b \cdot T + c \cdot T^2) + 0.38 \cdot u_{\mathrm{av}}^2 \right] \cdot \left(\frac{Sc}{660} \right)^{-0.5} \tag{2-3}$$

where a, b, and c are empirical constants, taking values of 0.5246, 1.6256×10^{-2}, and 4.9946×10^{-4}, respectively, l is a scaling constant of value 2.778×10^{-6}, T is the temperature in °C, u_{av} is the long-term average wind speed (m s^{-1}), and Sc is the Schmidt number for CO_2 in sea water, which can be approximated by

$$Sc = a - b \cdot T + c \cdot T^2 - d \cdot T^3 \tag{2-4}$$

where a, b, c, and d are empirical constants, taking values of 2073.1, 125.62, 3.6267, and 0.043219, respectively [*Wanninkhof*, 1992].

In order to calculate the net exchange of CO_2 between the atmosphere and ocean, assuming that sea ice represents an impenetrable barrier to gaseous diffusion [*Sarmiento et al.*, 1992] the flux density across the air-sea interface is simply multiplied by the ice-free area, and summed over all grid points

$$F^{CO_2}_{air\rightarrow sea} = \sum_c \left(f^{CO_2}_{air\rightarrow sea(c)} \cdot \left(A_{(c)} - A_{ice(c)} \right) \right) \quad (2\text{-}5)$$

Where $A_{(c)}$ and $A_{ice(c)}$ are the appropriate total and sea ice areas, respectively, corresponding to grip point *c*.

2.2.2.2 Ocean-atmosphere O_2 exchange

Unlike CO_2, dissolved oxygen concentrations ($[O_2]$) are not buffered by the presence of a complex chemical reservoir so that $[O_2]$ in the surface ocean is often close to equilibrium with the atmosphere. The simplifying assumption is therefore often made in carbon cycle models that strict equilibrium is always maintained [*Bolin et al.*, 1983; *Maier-Reimer*, 1993; *Yamanaka and Tajika*, 1996]. However, this doesn't necessarily hold true in regions where vigorous convective overturning takes place such that the residence time of water at the surface may be too short for full equilibration with the atmosphere to take place [*Heinze et al.*, 1999]. A simple restoring scheme is therefore adopted, weighted by the fractional ice-free area

$$[O_2]_{new} = [O_2]_{old} + \frac{\left(A_{tot} - A_{ice} \right)}{A_{tot}} \cdot ([O_2]_{eqm} - [O_2]_{old}) \cdot \frac{\Delta t}{\tau_{O_2}} \quad (2\text{-}6)$$

where $[O_2]_{new}$ is the new concentration of dissolved O_2 after exchange with the atmosphere, $[O_2]_{old}$ is the old value before any exchange, and $[O_2]_{eqm}$ is the theoretical concentration of O_2 in the ocean in equilibrium with an atmospheric partial pressure ($pO_{2(atm)}$) of 0.2096 atm, given by

$$[O_2]_{eqm} = Q_{O_2(T,S)} \cdot pO_{2(atm)} \quad (2\text{-}7)$$

where $Q_{O_2(T,S)}$ is the Henry's Law constant for O_2 as a function of temperature and salinity in the surface ocean [*Millero and Sohn*, 1992]. The model time step is Δt, with τ_{O_2}, the restoring time for $[O_2]$ assigned a default value of 30 days.

2.2.3 Biological new production

Numerous mechanistic schemes for representing biological productivity in the surface ocean based on a multi-component description of ecosystem structure and nutrient cycling have been developed to date [*Aksnes et al.*, 1995; *Andersen et al.*, 1987; *Fasham et al.*, 1990]. These range in complexity from single nutrient and single phytoplankton component systems operating within a homogeneous surface ocean layer, to systems of multiple nutrients and trophic levels, all coupled to a 1D physical model. The export flux of particulate biogenic matter out of the surface layer in these models is derived from primary productivity taking into account various recycling and transformation processes within the euphotic zone. Although such schemes have been incorporated into global carbon cycle models their computational demands make their use in extended model runs problematic. In addition, they are often not particularly generalized and may require site-specific tuning [*Hurtt and Armstrong*, 1996, 1998].

Much simpler is to attempt to estimate new (export) production directly from available surface nutrient concentrations, a tactic used in many carbon cycle models. Of limited use in addressing the glacial-interglacial question in this regard are schemes where export production is calculated to effectively 'restore' surface ocean nutrient concentrations to some pre-determined value (e.g., *Marchal et al.* [1998b], *Murnane et al.* [1999], *Najjar et al.* [1992]). Alternatively, export production may be parameterized as a function of a single nutrient (usually PO_4), modified by terms representing Michaelis-Menten kinetic nutrient limitation, together with some or all of light, temperature, and mixed layer depth [*Bacastow and Maier-Reimer*, 1990; *Heinze et al.*, 1991; *Maier-Reimer*, 1993]. Recently, the effect of additional limiting nutrients (H_4SiO_4 and Fe) have also been considered [*Archer and Johnson*, 2000; *Archer et al.*, 2000; *Henize et al.*, 1999; *Lefèvre and Watson*, 2000; *Watson et al.*, 2000]. However, common to all of these schemes is the calculation of a single value of whole-community organic carbon export. While this is sufficient in terms of the organic carbon pump alone, $CaCO_3$ and opal production remain to be estimated. The magnitude of $CaCO_3$ export flux together with its 'rain ratio' with respect to particulate organic carbon (POC), plays a critical role in controlling the alkalinity balance of the ocean and thus in determining xCO_2 [*Archer and Maier-Reimer*, 1994]. For this reason it is undesirable to assume an invariant ratio of $CaCO_3$:POC new production over the glacial-interglacial cycles. Not only is reproducing the observed spatial heterogeneity in rain ratios (at least to a first order) a precondition for effective simulation of Holocene sediments, being able to account for differences in this ratio during glacial times facilitates verification of the mechanism(s) assumed for glacial-interglacial change through comparisons between observed and model Last Glacial Maximum (LGM) sediment distributions. Similar arguments also apply for opal:POC. Unfortunately, since ecosystem structure is fundamental in determining such ratios there is no simple means of deriving their values from a total POC flux [*Shaffer*, 1993], although (highly parameterized) attempts have been made taking into account ambient nutrient and temperature conditions [*Archer et al.*, 1999a,b, 2000; *Heinze et al.*, 1999; *Maier-Reimer*, 1993].

A new computationally-efficient scheme for surface ocean biological production is presented here. In the manner in which it seeks to estimate export production out of the euphotic zone directly from surface physical and chemical conditions (as opposed to via a full ecosystem model) it is similar to that of *Maier-Reimer* [1993]. However, a significant departure is made in that production arising from two distinct classes of phytoplankton is considered; siliceous phytoplankton ("SP") and non-siliceous phytoplankton ("NSP"), following *Egge and Aksnes* [1992]. SP (typified by open ocean diatom species such as *Thalassiosira oceanica*) are assumed to be solely responsible for the production of opal, and as a result are limited by the availability of H_4SiO_4. In contrast, NSP (typified by open ocean coccolithophorids

such as *Emiliania huxleyi*, but including the bulk of pico- and nano-phytoplankton species), have no such silicic acid limitation and are assumed to be the sole producers of $CaCO_3$. Both classes are affected by ambient $[PO_4]$ and [Fe], temperature, and light. In the absence of any nutrient limitation (and assuming a stable water column and adequate insolation levels) siliceous phytoplankton tend to dominate the phytoplankton community [*Egge*, 1998]. SP are therefore characterized in the model by a relatively high (export) productivity. NSP tend to generally comprise somewhat smaller species with productivity much more tightly controlled by grazing, and are therefore characterized by relatively low productivity. Obviously this is highly simplistic, with no explicit representation of the role played by zooplankton or of the microbial loop [*Taylor and Joint*, 1990]. In addition, the important contribution made to POC export in regions such as the Southern Ocean by high productivity non-siliceous bloom-forming species such as *Phaeocystis antarctica* [*Elderfield and Rickaby*, 2000] will not be captured. However, such a scheme is still able to capture the first order contrast in the observed $CaCO_3$:POC rain ratio between different oceanic regions as will be demonstrated later (4.4.2).

Although the biological scheme is based around nutrient limitation by PO_4, H_4SiO_4, and Fe, present-day surface nutrient distributions suggests that the availability of nitrate (NO_3) is likely to be generally more limiting to phytoplankton growth than PO_4 [*McElroy*, 1983; *Tyrrell*, 1999]. However, considering the complexity of the oceanic NO_3 cycle no explicit representation is incorporated in SUE at present, although account is still taken of the contribution made to alkalinity partitioning in the ocean by NO_3 cycled through the 'soft tissue pump' [*Broecker and Peng*, 1982].

2.2.3.1 Phosphate uptake model

Net uptake fluxes (in units of mol PO_4 kg^{-1} a^{-1}) within the euphotic zone by siliceous phytoplankton ($u_{SP}^{PO_4}$) and non-siliceous phytoplankton ($u_{NSP}^{PO_4}$) are based upon the 'law of the minimum' for multiple nutrient limitation [*Aksnes et al.*, 1994], and described by

$$u_{SP}^{PO_4} = u_{0,SP}^{PO_4} \cdot \mathrm{MIN}\left(k_{SP}^{PO_4}, k_{SP}^{H_4SiO_4}, k_{SP}^{Fe}\right) \cdot \mu_{(I)} \cdot \mu_{(T)} \quad (2\text{-}8a)$$

$$u_{NSP}^{PO_4} = u_{0,NSP}^{PO_4} \cdot \mathrm{MIN}\left(k_{NSP}^{PO_4}, k_{NSP}^{Fe}\right) \cdot \mu_{(I)} \cdot \mu_{(T)} \quad (2\text{-}8b)$$

where $u_{0,SP}^{PO_4}$ and $u_{0,NSP}^{PO_4}$ are uptake rates (mol PO_4 kg^{-1} a^{-1}) in the absence of any nutrient limitation for SP and NSP, respectively, and treated as optimizable parameters. $\mu_{(I)}$ is a factor accounting for the effects ambient solar insolation has on new production, while $\mu_{(T)}$ is similar, but for temperature. A realistic treatment of light limitation is complex, requiring consideration of the depth distribution of phytoplankton in the water column, effects of self-shading and photo-inhibition, and an estimate of the depth of the mixed layer [*Andersen et al.*, 1987; *Taylor et al.*, 1991; *Tyrrell and Taylor*, 1996], all of which are beyond the scope of the current model. A simple (normalized) insolation factor is therefore used (detailed in Appendix II). $\mu_{(T)}$ is defined

$$\mu_{(T)} = e^{(a \cdot T)} \quad (2\text{-}9)$$

such that $\mu_{(T)}$ takes a value of unity at a temperature of 0°C. A Q_{10}-type dependence is assumed, with the scalar a given by [*Aksnes et al.*, 1995]

$$a = \ln\left(\frac{Q_{10}}{10}\right) \quad (2\text{-}10)$$

Following *Eppley* [1972] Q_{10} for phytoplankton growth of 1.88 is assumed, giving $a = 0.063$. No distinction is made between the two phytoplankton groups in terms of their temperature response [*Aksnes et al.*, 1995].

The '*k*' terms in (2-8a) represent Michaelis-Menten kinetic limitation of uptake [*Aksnes and Egge*, 1991; *Dugdale*, 1967]

$$k_{SP}^{PO_4} = \frac{[PO_4]}{K_{S,SP}^{PO_4} + [PO_4]} \quad (2\text{-}11)$$

$$k_{SP}^{H_4SiO_4} = \frac{[H_4SiO_4]}{K_{S,SP}^{H_4SiO_4} + [H_4SiO_4]} \quad (2\text{-}12)$$

$$k_{SP}^{Fe} = \frac{[Fe]}{K_{S,SP}^{Fe} + [Fe]} \quad (2\text{-}13)$$

where K_S values in the three equations are the half-saturation constants for the respective nutrients. The NSP terms are similar, except that there is no H_4SiO_4 limitation.

Strictly speaking, Michaelis-Menten limitation kinetics and the associated use of half-saturation constants are not directly applicable to a model of this type. Reported constants are calculated on the basis of growth rate of individual phytoplankton cells, whereas SUE seeks to predict net nutrient removal throughout the euphotic zone (and with it, export production). It is likely that export production has no simple relationship with primary production. Indeed, a tendency for export production to increase more rapidly with increasing primary production than primary production itself has been reported [*Aksnes and Wassmann*, 1993]. However, for want of a suitable alternative, this concise and easily interpretable parameterization is adopted for the purpose of this resent study.

Integrating net uptake ((2-8a) and (2-8b)) over the depth of the euphotic zone (D_{euph}) and total ice free area gives the total net uptake rate from each oceanic region (in units of mol PO_4 a^{-1})

$$U_{SP}^{PO_4} = u_{SP}^{PO_4} \cdot 1027 \cdot \left(1 - \left(A_{tot} - A_{ice}\right)\right) \cdot D_{euph} \quad (2\text{-}14a)$$

$$U_{NSP}^{PO_4} = u_{NSP}^{PO_4} \cdot 1027 \cdot \left(1 - \left(A_{tot} - A_{ice}\right)\right) \cdot D_{euph} \quad (2\text{-}14b)$$

where the mean density of sea water is assumed to be 1027 kg m^{-3}. Finally, (steady state) export production out of the euphotic zone is simply equal to net uptake. Partitioning this export into particulate (POP) and dissolved organic phosphate (DOP) forms, gives

$$Fnp_{SP}^{POP} = \lambda_{SP} \cdot U_{SP}^{PO_4} \quad (2\text{-}15a)$$

$$Fnp_{NSP}^{POP} = \lambda_{NSP} \cdot U_{NSP}^{PO_4} \quad (2\text{-}15b)$$

and

$$Fnp_{SP}^{DOP} = (1 - \lambda_{SP}) \cdot U_{SP}^{PO_4} \quad (2\text{-}16a)$$

$$Fnp_{NSP}^{DOP} = (1 - \lambda_{NSP}) \cdot U_{NSP}^{PO_4} \quad (2\text{-}16b)$$

Where λ_{SP} and λ_{NSP} are the export partitioning coefficients for SP and NSP, respectively.

2.2.3.2 Nutrient half-saturation constants

Phytoplankton nutrient half saturation constants are derived from values observed in both incubation and whole-ocean ecosystem studies. These values are summarized in Table 2-1, and adopted on the following basis

Phosphate

The PO_4 half saturation constant for siliceous phytoplankton ($K_{S,SP}^{PO_4}$) is taken from the diatom value used by *Aksnes et al.* [1995]. Coccolithophorids have been observed to exhibit a higher affinity for phosphate than do diatoms [*Aksnes et al.*, 1994; *Egge* 1998]. The PO_4 half saturation constant for non-siliceous phytoplankton ($K_{S,NSP}^{PO_4}$) is therefore assigned a value some 50% lower than that assumed for siliceous phytoplankton in order to reflect this difference.

Silicic acid

The half-saturation constant for siliceous phytoplankton is taken to be 4 μmol kg^{-1}, consistent with kinetic experiments on single and diatoms and natural assemblages suggest a value for $K_{S,SP}^{H_4SiO_4}$ in the range 0.5-5.0 μmol kg^{-1} [*Dugdale et al.*, 1995; *Officer and Ryther*, 1980].

Iron

Assigning globally representative half-saturation constant values for Fe is much more problematic than for the macro-nutrients. While *Sunda and Huntsman* [1995] reported K_S^{Fe} values for several typical oceanic diatom species, their experimental system was heavily EDTA-buffered with results reported on a calculated dissolved Fe^{II} scale. It is unwise to utilize the results of such a system directly [*Gerringa et al.*, 2000; *Muggli et al.*, 1996]. More applicable are results of Fe additions made to natural systems when the concentration of Fe tends to be operationally defined and thus substantially equivalent to the total dissolved Fe scale considered in SUE. Incubation enrichment experiments on equatorial Pacific samples indicate a whole-community K_S^{Fe} of 0.12 nmol kg^{-1} [*Coale et al.*, 1996b; *Fitzwater et al.*, 1996], while similar experiments conducted at the equator and 15°N are consistent with values of 0.035 and 0.22 nmol kg^{-1}, respectively [*Price et al.*, 1994]. More recent enrichment incubation experiments carried out by *Takeda* [1998] are consistent with a value for K_S^{Fe} of 0.25-0.75 nmol kg^{-1} for oceanic waters of all three main HNLC zones, while *Hutchins and Bruland* [1998] suggest values characterizing the California coastal up-welling regime lie anywhere in the range 0.02-1.0 nmol kg^{-1} (depending on the precise details of the operational definition of [Fe] chosen). A value of $K_{S,dia}^{Fe}$ of 0.125 nmol kg^{-1} is therefore chosen generally consistent with these estimates and assuming that most of the observed changes in primary production is due to diatoms. On the basis that *Sunda and Huntsman* [1995] observed half-saturation values for *T. oceanica* approximately twice that for *E. huxleyi*, $K_{S,NSP}^{Fe}$ is taken to be 50% lower than that of $K_{S,SP}^{Fe}$.

Table 2-1 Nutrient Half-saturation Values for the Two Phytoplankton Groups Considered in SUE

Phytoplankton group	Nutrient	K_S value
Siliceous	PO_4	0.1 μmol kg^{-1}
Siliceous	H_4SiO_4	4.0 μmol kg^{-1}
Siliceous	Fe	0.125 nmol kg^{-1}
Non-siliceous	PO_4	0.05 μmol kg^{-1}
Non-siliceous	H_4SiO_4	n/a
Non-siliceous	Fe	0.0675 nmol kg^{-1}

2.2.3.3 'Redfield' and derived chemical export ratios

While (2-15a) and (2-15b) together predict particulate PO_4 export from the euphotic zone the export of other biogeochemically important nutrient and non-nutrient chemical species, such as H_4SiO_4, Fe, CO_2, and alkalinity (from Ca^{2+} and NO_3^-) must now be derived. The organic or inorganic components of particulate matter export are related directly (or via an intermediary) to phosphate export, by a series of characteristic ratios. For SP, these relationship are

$$Fnp_{SP}^{POC} = r_{SP}^{POC:POP} \cdot Fnp_{SP}^{POP} \quad (2\text{-}17)$$

$$Fnp_{SP}^{ALK} = -0.7 \cdot r_{SP}^{PON:POP} \cdot Fnp_{SP}^{POP} \quad (2\text{-}18)$$

$$Fnp_{SP}^{POFe} = r_{SP}^{POFe:POC} \cdot Fnp_{SP}^{POC} \quad (2\text{-}19)$$

$$Fnp_{SP}^{opal} = r_{SP}^{opal:POC} \cdot Fnp_{SP}^{POC} \quad (2\text{-}20)$$

where $r_{SP}^{x:y}$ is a molar ratio linking constituent x to y. For NSP, they are

$$Fnp_{NSP}^{POC} = r_{NSP}^{POC:POP} \cdot Fnp_{NSP}^{POP} \quad (2\text{-}21)$$

$$Fnp_{NSP}^{ALK} = -0.7 \cdot r_{NSP}^{PON:POP} \cdot Fnp_{NSP}^{POP} + 2 \cdot r_{NSP}^{CaCO_3:POC} \cdot Fnp_{NSP}^{POC} \quad (2\text{-}22)$$

$$Fnp_{NSP}^{POFe} = r_{NSP}^{POFe:POC} \cdot Fnp_{NSP}^{POC} \quad (2\text{-}23)$$

The proportions of C and N to P in POM are characterized by observed mean ratios (the so-called 'Redfield' ratios), with $r^{POC:POP}$ and $r^{PON:POP}$ taking values of 106:1 and 16:1, respectively [*Redfield et al.*, 1963]. The same ratios are assumed for POM derived from both SP and NSP. Net oxygen production in the euphotic zone is assumed to be in a fixed ratio to phosphate export, with O_2:P of 177:1.

Recent studies have indicated profound physiological effects on phytoplankton of iron availability aside from the direct influence on growth rate. For instance, phytoplankton have been observed to take up Fe in an apparent 'luxuriant' manner when ambient Fe availability is high [*Sunda et al.*, 1991; *Sunda and Huntsman*, 1995]. A second physiological change manifests itself through the molar ratio of cellular carbon to frustular opal in diatoms, with the apparent efficiency of silicic acid utilization (per unit carbon fixed) increasing with iron availability. Where available H_4SiO_4 is limiting to diatom growth, therefore, enhanced iron supply may enable increased diatom organic carbon export without any concurrent increase in opal export. This has important implications both for the operation of the global carbon cycle and for the paleoclimatic interpretation of sedimentary opal content and accumulation rates in deep sea sediment cores [*Anderson et al.*, 1998; *Boyle*, 1998; *Takeda*, 1998; *Watson et al.*, 2000]. The export ratios $r_{SP}^{POFe:POC}$, $r_{NSP}^{POFe:POC}$, and $r_{SP}^{opal:POC}$ are therefore defined as functions of Fe availability. Although Fe availability was previously thought to have relatively little influence on the ratios linking C, N, and P [*Greene et al.*, 1991], nitrate utilization appears to be significantly greater per unit carbon fixed under Fe-replete conditions [*Cullen,* 1995; *Hutchins and Bruland*, 1998; *Hutchins et al.*, 1998; *Muggli et al.*, 1996; *Takeda*, 1998]. Since there is no explicit consideration of NO_3 in SUE and little quantitative information is currently available concerning changes in H_4SiO_4:PO_4 uptake, no dependence of [Fe] on either $r^{POC:POP}$ or $r^{PON:POP}$ is considered.

Export $CaCO_3$:POC ratio

The export ratio of $CaCO_3$:POC from non-siliceous phytoplankton ($r_{NSP}^{CaCO_3:POC}$) is left as an optimizable parameter in the model. $CaCO_3$ in SUE is resolved in calcitic and aragonitic components. Although there is little available data for aragonite export, sediment trap measurements suggest that aragonite constitutes at least 12% of the total $CaCO_3$ sinking flux at a depth of 667 m in the equatorial Atlantic [*Berner and Honjo*, 1981], but can be as high as 24% at 100 m in the North Pacific [*Betzer et al.*, 1984]. Aragonite is therefore assumed to constitute ~5% of $CaCO_3$ export production, equivalent to ~10% at 1000 m depth as a result of rapid reduction in calcite fluxes through the mesopelagic zone (see 2.2.4.2).

While the value of $r_{NSP}^{CaCO_3:POC}$ is itself invariant and spatially uniform the overall, $CaCO_3$:POC export ratio comprises export from both SP (contributing POC only) and NSP (contributing both POC and $CaCO_3$). Temporal or spatial variability in the balance between SP and NSP productivity (for instance, due to changes in the availability of H_4SiO_4) can thus give rise to variability in the net $CaCO_3$:POC export ratio.

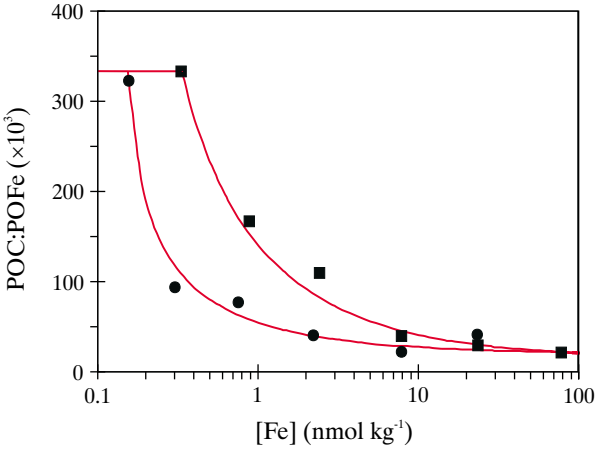

Figure 2-2 Model relationship for the export ratio of POC:POFe (i.e., the reciprocal of $r^{POFe:POC}$), for both siliceous phytoplankton (upper line) and non-siliceous phytoplankton (lower line) as functions of the concentration of total dissolved iron ([Fe]). Observational data for *T. oceanica* (filled squares) and *E. huxleyi* (filled circles) are from *Sunda and Huntsman* [1995].

Export POC:POFe ratio

Export POFe:POC ratios are related to Fe availability empirically in the model based on culture results reported by *Sunda and Huntsman* [1995]. Their theoretical free Fe^{II} (Fe′) scale is converted to the equivalent in total dissolved iron ([Fe]) used in SUE by assuming that the half saturation constant for diatoms on the [Fe′] scale of ~0.004 nmol kg^{-1} [*Sunda and Huntsman*, 1995], can be equated directly to the estimated value for NSP of 0.125 nmol kg^{-1} of [Fe] derived earlier (2.2.3.2). A simple power law function is used, with the observed behaviour of *T. oceanica* taken to be representative of SP, and *E. huxleyi* of NSP [*Sunda and Huntsman*, 1995]. Assuming that there is no fractionation between Fe and C components of POM primary production within the euphotic zone, Fe:C export ratios for the two phytoplankton groups are set equal to these cellular relationships. A threshold level is imposed and set at the maximum observed efficiency of iron utilization [*Sunda and Huntsman*, 1995]; a value of some 3 μmol Fe (mol C)$^{-1}$ for both $r_{SP}^{POFe:POC}$ and $r_{NSP}^{POFe:POC}$. The relationships thereby obtained (Figure 2-3) are

$$r_{SP}^{POFe:POC} = \frac{1}{\mathrm{MIN}\left(333000,\ 15000 + 115623 \cdot ([Fe] - 0.125)^{-0.65}\right)} \quad (2\text{-}24a)$$

and

$$r_{SP}^{POFe:POC} = \frac{1}{\mathrm{MIN}\left(333000,\ 20000 + 31805 \cdot ([Fe] - 0.125)^{-0.65}\right)} \quad (2\text{-}24b)$$

where [Fe] is the total dissolved iron concentration in units of nmol kg^{-1}.

Export opal:POC ratio

Incubation and ocean patch studies have reported changes in the cellular uptake ratios of H_4SiO_4:C and H_4SiO_4:NO_3 by HNLC-type phytoplankton assemblages upon the addition of iron [*Hutchins and Bruland*, 1998; *Takeda*, 1998; *Watson et al.*, 2000], summarized in Table 2-2. Fe-stressed diatoms are also visibly more heavily silicified [*Hutchins et al.*, 1998; *Leynaert et al.*, 1993]. This increase in diatom H_4SiO_4:C with decreasing Fe-availability has been suggested to be due to the order of cell cycle events, where silicic acid uptake only occurs in a phase just prior to cellular division [*Pondaven et al.*, 1999]. If division is delayed through Fe-limitation, the length of time available for opal deposition is longer, thus resulting in a higher degree of diatom silicification. If this is the case, a reasonable starting point in relating H_4SiO_4:C uptake to ambient [Fe] would be to assume that this ratio is proportional to Fe-stress as defined by the reciprocal of the relevant Michaelis-Menten kinetic term (2-16), to give

$$r_{SP}^{H_4SiO_4:C} = r_{0,SP}^{H_4SiO_4:C} \cdot \frac{1}{k^{Fe}} \qquad (2\text{-}25)$$

where $r_{0,SP}^{H_4SiO_4:C}$ is the ratio of H_4SiO_4:C uptake under Fe-replete conditions. The singularity at [Fe] = 0 is removed by adding a fixed offset ($[Fe]_{off}$) to the value of ambient [Fe]. The observed decrease in diatom H_4SiO_4:C with increasing Fe availability (Table 2-3) can be reasonably reproduced with K_S^{Fe} = 0.25 nmol kg^{-1}, and applying an offset in ambient [Fe] of 0.125 nmol kg^{-1}.

Given their very different biogeochemical natures, a high degree of differential recycling between opal and POC within the euphotic zone is likely [*Dugdale et al.*, 1995; *Dugdale and Wilkerson*, 1998]. Changes in the degree of diatom silicification may alter the magnitude of this differential, such as through changes in sinking rate [*Boyle*, 1998; *Muggli et al.*, 1996], grazing susceptibility, or the 'quality' of frustuline opal (and thus solubility and/or dissolution rate). However, for simplicity the export opal:POC ratio ($r_{SP}^{opal:POC}$) will be assumed to scale linearly with the cellular H_4SiO_4:C uptake ratio. The export ratio can therefore be written

$$r_{SP}^{opal:POC} = r_{0,SP}^{opal:POC} \cdot \frac{K_S^{Fe} + ([Fe] + [Fe]_{off})}{([Fe] + [Fe]_{off})} \qquad (2\text{-}26)$$

where $r_{0,SP}^{opal:POC}$ is now the export opal:POC ratio under Fe-replete conditions. The form of this relationship is shown in Figure 2-3. The magnitude of differential recycling within the euphotic zone represented by the implicit scale factor linking $r_{0,SP}^{opal:POC}$ to $r_{0,SP}^{H_4SiO_4:C}$ is poorly quantified, and has been variously estimated to be in the range 1.25 to 3.0 depending on assumptions made regarding grazing [*Dugdale et al.*, 1995; *Dugdale and Wilkerson*, 1998]. $r_{0,SP}^{opal:POC}$ is therefore left as an optimizable parameter in the model.

Table 2-2 Observed Dependence of Molar Uptake Ratios upon Iron Availability

Identifier and location	Treatment	[Fe] (nmol kg^{-1})	H_4SiO_4: NO_3^-	H_4SiO_4: C	Growth rate (d^{-1})	Reference
#1 - Big Sur 1997A	Control	0.1-0.5 [1]	1.6	0.27	0.30	*Hutchins and Bruland* [1998]
	Fe addition	2.5	0.8	0.21	0.68	
#2 - Big Sur 1996	Control	0.06-0.3 [1]	2.7	0.39	0.70	*Hutchins and Bruland* [1998]
	Fe addition	10	1.1	0.24	0.94	
#3 - Ano Nuevo 1995	Control	1.5-2.6 [1]	1.0	n/a	0.44	*Hutchins and Bruland* [1998]
	Fe addition	10	0.9	n/a	0.37	
#4 - Southern Ocean	Control	0.16	2.3	n/a	0.13	*Takeda* [1998]
	Fe addition	1.2	0.95	n/a	0.43	
#5 - Subarctic North Pacific	Control	0.22	2.6	n/a	0.14	*Takeda* [1998]
	Fe addition	1.1	1.2	n/a	0.49	
#6 - Equatorial Pacific	Control	<0.05	1.3	n/a	0.06	*Takeda* [1998]
	Fe addition	0.46	0.45	n/a	0.48	
	Fe addition	0.72	0.45	n/a	0.79	
#7 - Southern Ocean	Control	0.06	n/a	0.36±0.015	n/a	*Watson et al.* [2000]
	Fe addition	0.3-3.0 [2]	n/a	0.18±0.1	n/a	

[1] Control Fe concentration are presented as a range of estimates, depending on the analytical method employed [*Hutchins and Bruland*, 1998].

2.2.4 Remineralization within the water column

Much of particulate biogenic material exported out of the euphotic zone is remineralized within the water column before it can reach the sediments. Material returned to solution in the mesopelagic zone has the potential to be rapidly returned to the surface, which in the case of nutrients such as PO_4, NO_3, H_4SiO_4, and Fe has obvious implications for surface productivity. The magnitude of the remaining particulate fraction reaching the sediments ultimately exerts an important control on oceanic inventories of nutrients, DIC, and ALK. An adequate representation of remineralization processes within the water column is therefore critical to any description of the global carbon cycle, particularly over glacial-interglacial time scales. In the following sections, a reference depth z_0 is defined at the base of the euphotic zone, where the settling flux of particulate constituent x is equal to the total export flux

$$Fset^{x}_{(z_0)} = Fnp^{x}_{SP} + Fnp^{x}_{NSP} \qquad (2.27)$$

For dissolved organic matter, remineralization proceeds according to a simple characteristic decay rate [*Marchal et al.*, 1998b; *Najjar et al.*, 1992] as it is transported though the ocean. No distinction is made between semilabile and refractory components [*Yamanaka and Tajika*, 1997].

2.2.4.1 Particulate organic matter

The processes involved in the remineralization of particulate organic matter (POM) within the water column are extremely complex, including such factors as the repackaging and aggregation/dispersal of particles, bacterial and zooplankton ecology and the occurrence of rapid export events following phytoplankton blooms [*Kriest and Evans*, 1999; *Shaffer*, 1993]. Simple empirical functions are therefore utilized in global carbon cycle models. Various schemes have been proposed, typically based on exponential [*Volk and Hoffert*, 1985] or power law [*Martin et al.*, 1987; *Suess*, 1980] functions in which the remaining (un-remineralized) fraction of the initial POM export flux is related directly to the depth in the water column. Of these, the parameterization of *Martin et al.* [1987], derived from a series of sediment trap measurements made during the 'VERTEX' programs and covering the uppermost 2000 m in the eastern equatorial Pacific tends to be fairly ubiquitous (e.g., *Maier-Reimer* [1993], *Yamanaka and Tajika* [1996]). However, sediment trap studies suggest that remineralization deeper than this is much less extensive than extrapolation of the *Martin et al.* [1987] function might suggest (Figure 2-4). Since any significant underestimation of POM rain rate to the sediments would reduce the component of $CaCO_3$ dissolution driven by *in situ* POM remineralization [*Archer and Maier-Reimer*, 1994] and thus disrupt global alkalinity, *Archer et al.* [1996, 1998] modified the *Martin et al.* [1987] function (Figure 2-4). Although this is in good agreement with deeper (> 2000 m) sediment trap observations, it tends to deviate a little from the VERTEX data at mesopelagic depths.

A slightly different function is adopted which assumes that a fraction of POM settles through the water column essentially unaltered, either due to rapid settling and/or a recalcitrant composition. The remaining fraction is degraded according to a simple power law. The settling flux of particulate organic phosphorous (POP) is therefore defined

$$Fset^{POP}_{(z)} = Fset^{POP}_{(z_0)} \qquad z \le z_0 \qquad (2.28a)$$

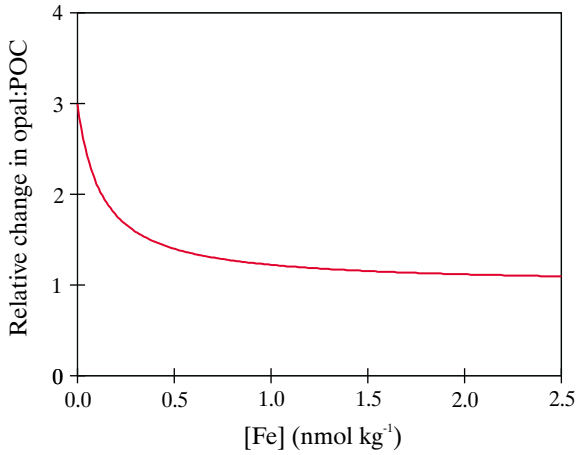

Figure 2-3 Change in siliceous phytoplankton opal:POC export relative to $r^{opal:POC}_{SP,0}$, as a function of the concentration of total dissolved iron ([Fe]).

Table 2-3 Observed and Model-estimated Relative Changes in H_4SiO_4:C Uptake From Comparatively Iron-deplete to Iron-replate Conditions

Identifier [1]	observed $\frac{H_4SiO_4:C_{deplete}}{H_4SiO_4:C_{replete}}$	model $\frac{H_4SiO_4:C_{deplete}}{H_4SiO_4:C_{replete}}$
#1	1.29	1.27-1.92 [2]
#2	1.63	1.59-2.35 [2]
#3	1.00 [3]	1.10-1.15 [2]
#4	1.58 [3]	1.58
#5	1.42 [3]	1.43
#6	1.89 [3]	>1.70 [4]
#7	2.00	2.03

[1] (see Table 2-2)

[2] Depending upon assumptions made regarding the exact value of [Fe] in the experimental control.

[3] Estimated from published changes in H_4SiO_4:NO_3^-. Care must therefore be taken in using these value, since there is also a significant dependence of H_4SiO_4:NO_3^- on [Fe].

[4] Assuming control [Fe] < 0.05 nmol kg^{-1}.

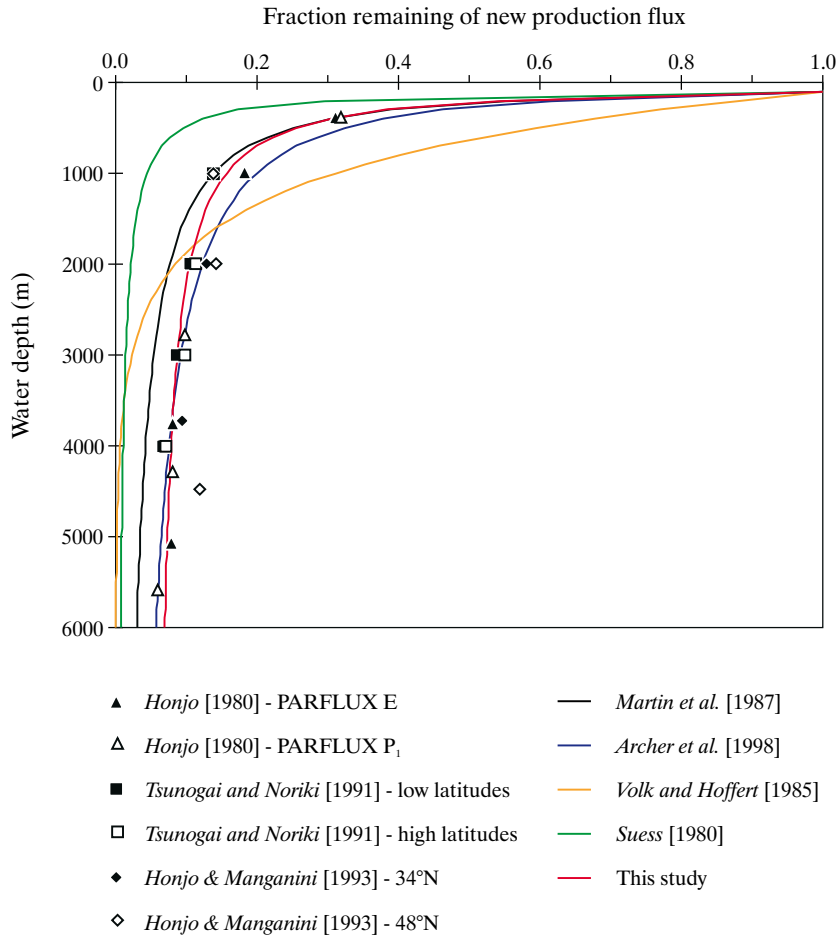

Figure 2-4 Model particulate organic matter remineralization profiles (solid lines) together with observed flux profiles (symbols). Observed profiles comprise a series of discrete flux measurements made by trap deployments over a range of depths. All profiles are normalized to unity at 100 m depth, which for measured profiles is carried out by assuming that the profile in between the shallowest available trap and 100 m depth obeys the *Martin et al.* [1987] curve.

$$Fset_{(z)}^{POP} = Fset_{(z_0)}^{POP} \cdot \left(0.05 + 0.95 \cdot \left(\frac{100 + (z - z_0)}{100}\right)^{-0.950}\right) \qquad z > z_0 \qquad (2.28b)$$

As shown in Figure 2-4, this gives a reasonable compromise solution, consistent with observations of both mesopelagic and bathypelagic flux profiles.

Constant ratios linking C, Fe, and N to P during the remineralization of POM are assumed throughout the water column, taking values equal to those characterizing mean export production (2-17 to 2-23). The remineralization of POM involves the oxidation of organic compounds, a process that requires the availability of oxygen (or an alternative electron donor). Dissolved oxygen is assumed to be depleted within the water column in a 177:1 molar ratio with the quantity of phosphate released. To prevent depletion of O_2 below zero in regions characterized by poor ventilation and/or high surface productivity, a minimum threshold is prescribed (taken to be 25 μmol kg^{-1}) below which no further depletion is allowed. POM continues to be remineralized in the model though, somewhat analogous to remineralization fuelled through denitrification (although nitrogen cycling is not explicitly represented).

2.2.4.2 Calcite

Calcite has been the only polymorph of $CaCO_3$ explicitly considered in global carbon cycle models to date. Its remineralization within the water column invariably proceeds in accordance with an exponentially decreasing flux profile, taking an *e*-folding depth sometimes as short as 2 km [*Heinze et al.*, 1999; *Maier-Reimer*, 1993], although studies where model alkalinity fields are fitted to observed data suggest a higher value in the region of 3-3.5 km [*Marchal et al.*, 1998b; *Yamanaka and Tajika*, 1996]. However, *Milliman et al.* [1999] concluded that 40-80% of $CaCO_3$ export dissolved at depths

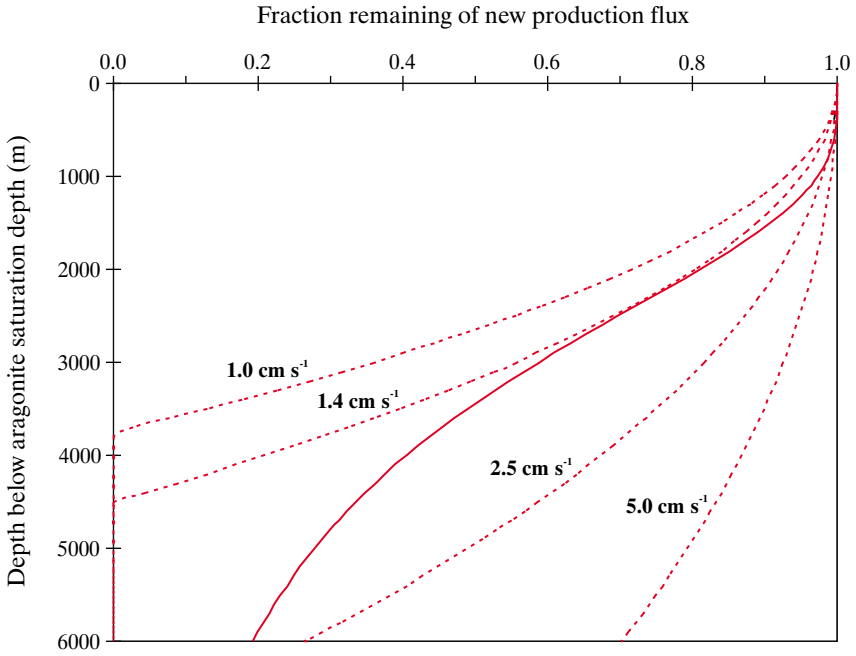

Figure 2-5 Aragonite remineralization profiles for; (a) initial size classes characterized by sinking rates of 1.0, 1.4, 2.5, and 5.0 cm s^{-1} [*Byrne et al.*, 1984] (dashed lines), (b) overall remineralization profile assuming an initial size distribution between these four classes of 2:2:3:3 (solid line).

shallower than about 1 km, while dissolution was inconsequential below this, perhaps due to the rapid dissolution of coccoliths in the guts of grazing zooplankton. This can be parameterized by the assumption of a fixed fraction of calcite export production with reaches the deep ocean without alteration, with the remainder subject to remineralization [*Archer et al.*, 1998]. The magnitude of the remineralizable fraction together with its remineralization scale length are chosen consistent with the general conclusions of *Milliman et al.* [1999], and more specifically, with the sediment trap observations of *Martin et al.* [1993] over the upper-most 1000 m. The calcite settling flux is therefore defined

$$Fset_{(z)}^{\text{calcite}} = Fset_{(z_0)}^{\text{calcite}} \qquad z \le z_0 \quad \text{(2-29a)}$$

$$Fset_{(z)}^{\text{calcite}} = Fset_{(z_0)}^{\text{calcite}} \cdot \left(0.4 + 0.6 \cdot e^{\left(\frac{-(z-z_0)}{500} \right)} \right) \qquad z > z_0 \quad \text{(2-29b)}$$

2.2.4.3 *Aragonite*

The remineralization of aragonite within the water column is based on the analysis of *Byrne et al.* [1984]. Their theoretical profiles of flux decrease with depth below the aragonite saturation horizon can be reasonably well fitted with a simple power function (Figure 2-5)

$$f_{(z)}^{\text{aragonite}} = f_{(z_{\text{sat}})}^{\text{aragonite}} \cdot \left(1 - \left(\frac{(z - z_{\text{sat}})}{z_l} \right)^2 \right) \qquad \text{(2-30)}$$

where $f_{(z)}^{\text{aragonite}}$ is the aragonite flux at depth z, $f_{(z_{\text{sat}})}^{\text{aragonite}}$ is the aragonite flux at the base of the photic zone, z_{sat} is the depth of the aragonite saturation horizon, and z_l is a scale depth for remineralization, depending on the initial size/settling rate. A net remineralization profile in the ocean can then be defined given the depth of the aragonite saturation horizon together with an estimate of the initial size distribution of sinking particles. Unfortunately, the latter piece of information is extremely poorly quantified. Aragonite export is therefore assumed to be comprised of a mixture of the four species considered by *Byrne et al.* [1984], *Culierina columnella*, *Limaclina bullmoldes*, *Limacina helicina*, and *Limacina inflata*. The initial export flux is partitioned 2:2:3:3 (by mass) between these, giving 40% of the flux as > 1 mm diameter particles, and 60% as < 500 μm, reasonably consistent with observations of aragonite flux size distributions [*Berner and Honjo*, 1981; *Bryne et al.*, 1984]. The remineralization of each initial class size is summed and the total flux fitted as a function of depth below the aragonite saturation horizon (Figure 2-5). The aragonite settling flux is therefore defined

$$Fset_{(z)}^{\text{aragonite}} = Fset_{(z_0)}^{\text{aragonite}} \qquad z \le z_{\text{sat}} \quad (2\text{-}31a)$$

$$Fset_{(z)}^{\text{aragonite}} = Fset_{(z_0)}^{\text{aragonite}} \cdot \left(1 - \left(\frac{(z - z_{\text{sat}})}{1000}\right)^{0.25} \cdot \left(1 - e^{\left(\left(\frac{-(z - z_{\text{sat}})}{1400}\right)^{4.5}\right)}\right)\right) \qquad z > z_{\text{sat}} \quad (2\text{-}31b)$$

2.2.4.4 Opal

In initial studies incorporating Si cycling into a global carbon cycle model the remineralization of opal within the water column was described with a simple exponential depth function, taking a somewhat arbitrary *e*-folding length of order 10 km [*Heinze et al.*, 1999; *Maier-Reimer*, 1993]. More recently, noting the importance of temperature in the control of dissolution rates, *Gnanadesikan* [1999] proposed a more realistic scheme. In this, the dissolution rate of opal, r^{opal} (d^{-1}) was described by

$$r^{\text{opal}} = 1.32 \times 10^{16} \cdot e^{\left(\frac{-11481}{T}\right)} \quad (2\text{-}32)$$

where T is the absolute temperature. Opaline particles were assumed to settle through the water column at a uniform rate of 50 m d^{-1}. While *Erez et al.* [1982] concluded that variations in silicic acid concentrations were not the main control on opal dissolution rates, this was on the basis of first-order dissolution kinetics, an assumption which has now been called into question [*Van Cappellen and Qiu*, 1997b]. A new scheme is therefore developed here, able to account explicitly for the dependence of opal remineralization of both ambient temperature and concentration of H_4SiO_4.

Model formulation

The description of opal remineralization is based empirically on the thermodynamic studies of *Van Cappellen and Qiu* [1997a,b] (see 3.2.5.1 for more details). Primary controls are assumed to be ambient temperature and the concentration of silicic acid, together with the settling velocity of the material. No account is taken of changes in surface reactivity which may occur during transit down through the water column, such as may arise through a general reduction in surface roughness or the removal of reactive sites at surface defects [*Van Cappellen and Qiu*, 1997b]. Bacteria may also play an important role in controlling the dissolution rate of diatom frustules, which strongly depends on the presence or absence of a protective organic coating [*Bidle and Azam*, 1999; *Kamatani*, 1982]. However, since the bacterial degradation of this layer appears to be substantially complete within a matter of only 1-2 days [*Bidle and Azam*, 1999], bacterial influence may be confined to pelagic and mesopelagic regions.

The rate of release of silicic acid within an ocean layer l resulting from the dissolution of biogenic opal settling through the water column, $Fdis_{(l)}^{\text{opal}}$ (mol a^{-1}), is described by

$$Fdis_{(l)}^{\text{opal}} = r_{(l)}^{\text{opal}} \cdot k_0^{\text{opal}} \cdot Fset_{(l)}^{\text{opal}} \cdot \Delta t_{(l)} \quad (2\text{-}33)$$

where k_0^{opal} is a base opal dissolution rate pertaining to ambient conditions of 0°C and complete under-saturation with respect to the solid phase, $Fset_{(l)}^{\text{opal}}$ is the settling flux of opal into the layer (mol a^{-1}), and $\Delta t_{(l)}$ is the residence time of this opal within the layer. $r_{(l)}^{\text{opal}}$ is a normalized dissolution rate (described in 3.2.5.1) characterized by a Q_{10} value of 2.3 for under-saturated conditions, consistent with the dissolution experiments of *Kamatani* [1982] and given by

$$r_{(l)}^{\text{opal}} = 0.225 \cdot \left(1 + \frac{T_{(l)}}{15}\right) \cdot u_{(l)}^{\text{opal}} + 0.775 \cdot \left(\left(1 + \frac{T_{(l)}}{400}\right)^4 \cdot u_{(l)}^{\text{opal}}\right)^{9.25} \quad (2\text{-}34)$$

where $u_{(l)}^{\text{opal}}$ is the degree of under-saturation of the solid phase (3.2.5.1).

The value for K_0^{opal} is derived from observed diatom dissolution rates. From laboratory studies, *Nelson et al.* [1976] found a mean dissolution rate in small centric diatoms under different growth conditions equivalent to 0.134 d^{-1} at 20°C, while two acid-washed coastal species (also measured at 20°C) dissolved at a rate of 0.074 d^{-1} [*Kamatani*, 1982]. Dissolution rates can also be estimated in the field from observations of the increase in sediment trap head-space [H_4SiO_4]. In this way, *Brzezinski and Nelson* [1995] calculated the dissolution rate of trapped material at 0.07 ± 0.03 d^{-1} at ~19°C, while *Blain et al.* [1999] estimated rates of 0.068 , 0.085 , 0.075, and 0.065 d^{-1} from a a series of four different deployment depths. If conditions of complete under-saturation (i.e., $u^{\text{opal}} = 1.0$) are assumed, and dissolution rates corrected to T = 0°C (estimated from *Levitus et al.* [1994c] where not reported) and taking a Q_{10} value of 2.3, a mean value across all these studies of 0.019 d^{-1} is obtained.

Analysis of sediment trap series suggests settling rates of opal material ranging from 32 to 200 m d^{-1} [*Blain et al.*, 1999; *Honjo and Manganini*, 1993; *Takahashi*, 1986]. In the absence of any tighter observational constraint a uniform sinking rate of 125 m d^{-1} is assumed following *Pondaven et al.* [1998]. The residence time $\Delta t_{(l)}$ (d) is then given by

$$\Delta t_{(l)} = \frac{th_{(l)}}{125} \quad (2\text{-}35)$$

where $th_{(l)}$ is the thickness (m) of the lth ocean layer.

Model evaluation

A number of studies have reported opal settling fluxes at multiple depths measured at the same geographical location, which in theory could be used to validate the remineralization model. However, there are a number of serious complications in the interpretation of opal sediment trap observations which are likely to significantly reduce their utility in such validation;

- Since the ocean is everywhere under-saturated with respect to biogenic opal, opal caught in sediment traps will continue to dissolve throughout the period of trap deployment. While recent studies make use of traps that

have been filled with high density brine solution in order to help quantify *in situ* dissolution (*Blain et al.* [1999]; *Brzezinski and Nelson* [1995]; *Honjo and Manganini* [1993]), early studies took no account of such losses (*Honjo* [1980]; *Noriki and Tsunogai* [1986]; *Takahashi* [1986]). Thus, account must be taken of the potential for the underestimation of settling fluxes by less sophisticated trap designs.

- Sinking fluxes may be modified by the random mesoscale eddy field through which the particles settle [*Siegel et al.*, 1990], an effect which can be manifested as an 'inverted' flux profiles (i.e., where measured fluxes *increase* with depth despite continued dissolution). Even where flux measurements have been made by free-floating traps (e.g., *Blain et al.* [1999]) there is likely to be some residual hydrodynamic distortion.
- Temporal variability in export production (such as associated with phytoplankton blooms) may cause problems in short term trap deployments. For instance, flux profiles which strongly increase with depth can arise should the traps be deployed at such a time that the uppermost trap samples post-bloom conditions while deeper ones still sample bloom conditions.
- In mesopelagic trap deployments, increased capture rates of radiolarians with depth may also produce inverted-type profiles [*Blain et al.*, 1999].
- Any decrease in surface reactivity as opal dissolves in the water column may lead to the influence of surface to deep contrasts in ambient temperature and $[H_4SiO_4]$ being overestimated. In particular, the microbial degradation of protective organic coatings on diatom frustules [*Bidle and Azam*, 1999; *Kamatani*, 1982] may significantly bias measurements made by near-surface trap deployments.

Studies reporting opal settling flux profiles used in the validation of the water-column dissolution model are detailed in Table 2-4 and the data shown in Figure 2-6. These data sets have been selected on the basis of there being no obvious distortion due to hydrodynamical or seasonal factors. For instance, some studies report a strongly increasing trend of $CaCO_3$ flux with depth [*Honjo*, 1980; *Honjo and Manganini*, 1993], suggestive of hydrodynamical distortion, while the character of the flux profile recorded by *Brzezinski and Nelson* [1995] associated with a bloom event was noticeably different to that observed during the remainder of the year. These are therefore omitted from further consideration.

Table 2-4 Biogenic Opal Flux Sediment Trap Data

Identifier	Location	Reference
#1	61.5°S, 150.5°E	*Noriki and Tsunogai* [1986]
#2	31.7°N, 124.6°W	*Noriki and Tsunogai* [1986]
#3	17.5°N, 117.0°W	*Noriki and Tsunogai* [1986]
#4	34°N, 21°W	*Honjo and Manganini* [1993]
#5	13°N, 54°W	*Honjo* [1980], *Honjo et al.* [1982]
#6	50°N, 145°W	*Takahashi* [1986]

The water column opal remineralization scheme (2-33) is run for each of the validation sites. Temperature and $[H_4SiO_4]$ profiles in the water column for these locations are taken from *Levitus et al.* [1994c] and *Conkright et al.* [1994], respectively. A base dissolution rate constant (K_0^{opal}) of 0.019 d^{-1} is assumed, along with a uniform settling rate of 125 m. The mean residence time of opal in the traps is taken to be equal to half of the total trap collection time. Opal dissolves continuously according to ambient conditions during this period and is assumed 'lost' in cases where the corresponding sediment trap measurements take no account of *in situ* dissolution. Predicted apparent settling fluxes (i.e., simulated measurements) are shown in Figure 2-6a. While the model is generally successful in approximating the apparent depth-invariance observed in many of the sediment trap studies, there are notable failures. Firstly, there is a pronounced intermediate-depth maximum in profile #2 whose magnitude is not well reproduced by the model. However, this profile can be reproduced by doubling the value of K_0^{opal} to 0.038, only slightly higher than the range of reported dissolution rates allow for. Secondly, dissolution in series #5 is seriously overestimated. In this case the profile can only be reproduced with a combination of lower values for both K_0^{opal} and settling velocity. Interestingly, the magnitude of the dissolution rate constant so required is similar to that observed from kinetic studies on core-top opal [*Van Cappellen and Qiu*, 1997b]. It is possible that the unusually long trap deployment period (98 days) [*Honjo*, 1980; *Honjo et al.*, 1982] might have resulted in geochemical conditions within the layer of accumulating trap material approaching that found in the benthic environment. If so, a combination of the presence of detrital silicate matter and local enrichment in ambient $[H_4SiO_4]$ may be acting so as to suppress the dissolution rate.

For comparison, the equivalent model predictions using the parameterization of *Gnanadesikan* [1999] are shown in Figure 2-6b. While some of the sediment trap data is consistent with this model over the upper most ~2500 m of the water column, there is a prominent negative trend with depth below this, contrary to observations. An improved fit is possible if a more rapid settling rate is adopted, although it is beyond this particular scheme's capability to fit either of data sets #2 and #5, regardless of assumptions made regarding settling rate.

Predicted opal remineralization profiles for the same six locations (Table 2-4) are shown in Figure 2-7. It can be seen that there are interesting regional contrasts in the degree of remineralization which occurs within the water column. The lowest degrees of remineralization are predicted for regions characterized by relatively low temperatures and high concentrations of silicic acid throughout the water column, such as found in the north Pacific (#6) and the Southern Ocean (#1). In contrast, a relative high degree of remineralization occurs throughout the water column in the low- and mid-latitude Atlantic (#4 and #5) where, despite temperatures rapidly decreasing with depth below the

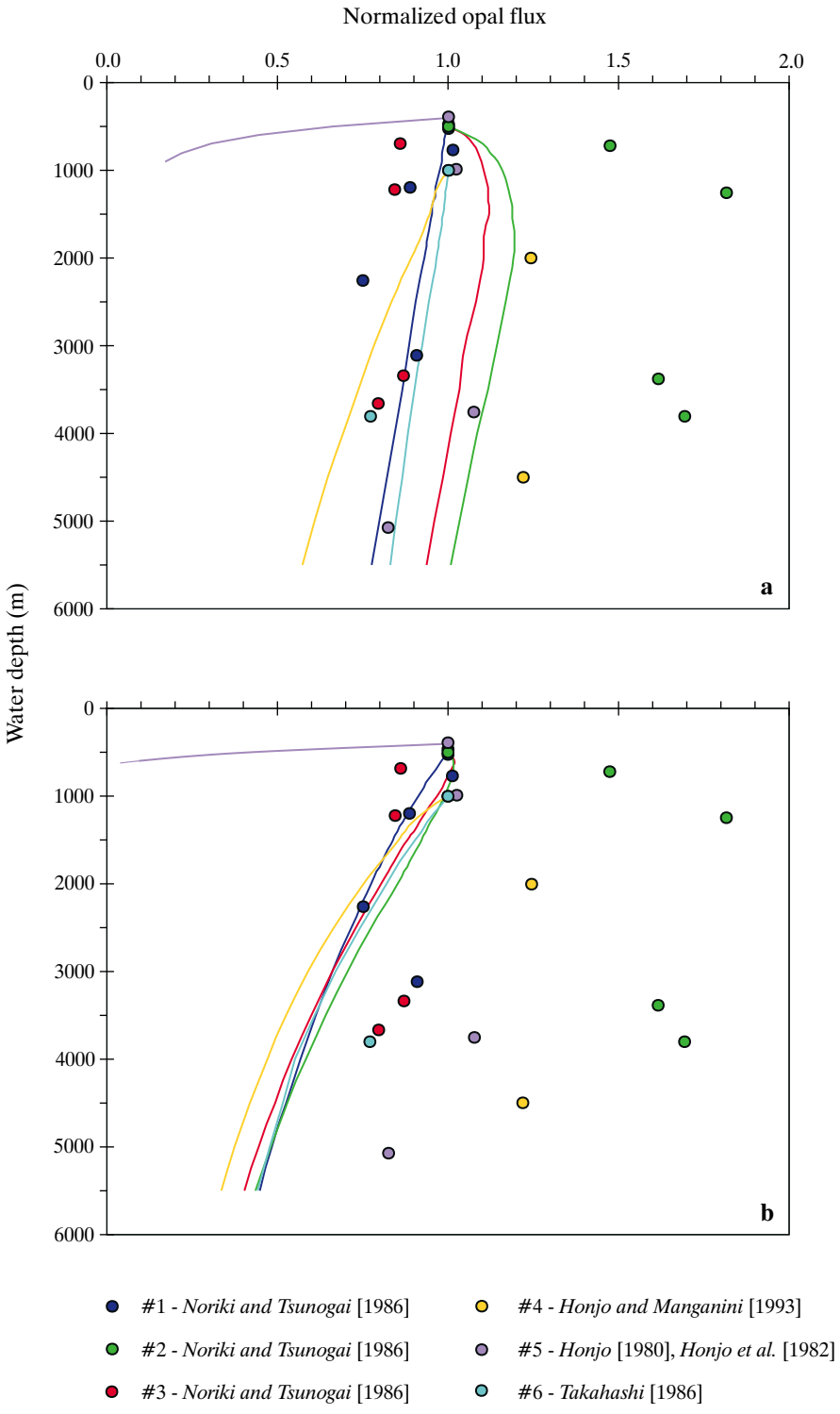

Figure 2-6 Apparent opal settling fluxes recorded by arrays of sediment traps, normalized to the value recorded in the uppermost trap of each array (filled symbols) and compared with model-predicted opal fluxes, normalized in a similar way (solid lines of a corresponding colour). Model results are shown for both the scheme developed here (a), and that of *Gnanadesikan* [1999] (b).

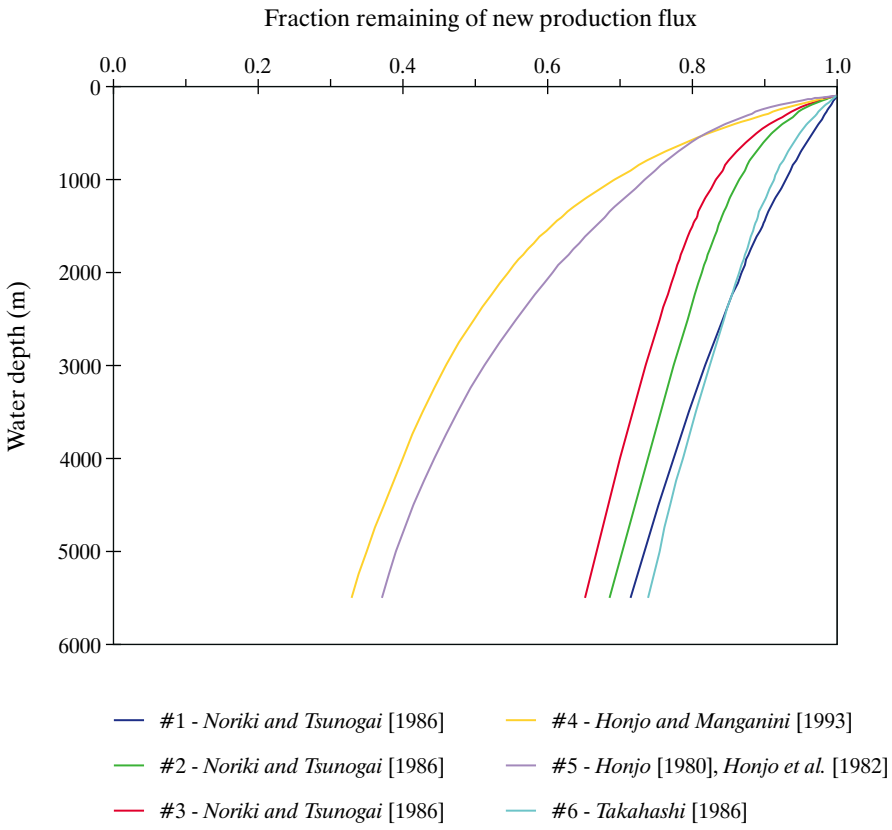

Figure 2-7 Model-predicted opal dissolution profiles, for each of the site locations detailed in Table 2-4. Opal rain rates are normalized to the flux at 100 m depth.

surface, $[H_4SiO_4]$ remains comparatively low and thus conditions highly under-saturated. Low- and mid-latitude Pacific regions (#2 and #3) are also characterized by high temperatures and low $[H_4SiO_4]$ at the surface. However, little remineralization occurs below the mesopelagic zone despite cold, high $[H_4SiO_4]$ deep ocean conditions.

2.2.5 Iron biogeochemical cycling

The behaviour of iron in the ocean is highly complex, involving transformations between various particulate, dissolved, and complexed phases [*Donaghay et al.*, 1991; *Johnson et al.*, 1997; *Gerringa et al.*, 2000]. The dynamic equilibrium state of such a system is strongly affected by such factors as *p*H [*Jickells*, 1999; *Jickells and Spokes*, in press; *Kuma et al.*, 1996], temperature, insolation levels [*Jickells and Spokes*, in press; *Kuma et al.*, 1996; *Sunda and Huntsman*, 1995], and the presence of organic compounds able to bind to Fe (ligands) [*Johnson et al.*, 1997; *Rue and Bruland*, 1997; *Sunda and Huntsman*, 1995]. Qualitative knowledge regarding the role of these (and further) factors is currently still in its infancy. SUE therefore considers a single 'total dissolved' iron phase, substantially equivalent to the operational definition in ocean Fe measurements [*de Baar and de Jong*, in press]. In this way, the values of Fe-related variables and parameters in the model should be directly comparable to those measured in both the ocean and laboratory seawater systems.

On the basis of the similarity between observed profiles of dissolved iron and nitrate in the upper 2000 m of the water column, the first-order biogeochemical behaviour of iron in the ocean has been considered to parallel that of other organic nutrients (PO_4 and NO_3) [*Johnson et al.*, 1997]. That is to say, like PO_4 and NO_3, Fe is taken up in a set ratio with carbon by phytoplankton (2-20, 2-23), exported as a component of (particulate) organic matter from the euphotic zone, and subsequently released back into dissolved form during remineralization within the water column. In common with other model studies [*Archer and Johnson*, 2000; *Lefèvre, and Watson*, 1999; *Watson and Lefèvre*, 1999], therefore, the basic biogeochemical scheme used for Fe follows that for PO_4. However, the extremely low solubility and high reactivity of free Fe in solution under typical seawater conditions results in it being readily scavenged out of

solution by the rain of particulate debris settling through the water column [*Johnson et al.*, 1997]. This scavenging has previously been represented by a simple characteristic residence time for dissolved Fe, assumed to be uniform in value throughout the ocean [*Archer and Johnson*, 2000; *Johnson et al.*, 1997; *Lefèvre and Watson*, 1999]. Intuitively, though, the scavenging rate should be directly related to the flux density of settling particulate material. SUE therefore scales local residence times inversely with particulate flux densities. Previous studies have also considered the ubiquitous presence of a Fe-binding ligand [*Archer and Johnson*, 2000; *Lefèvre and Watson*, 1999; *Watson and Lefèvre*, 1999], which acts so as to effectively prevent any further scavenging when Fe concentrations fall below that of the ligand [*Johnson et al.*,1997]. While the action of ligands in retaining Fe in solution, particularly in the surface ocean is undoubtably critical [*Rue and Bruland*, 1997], the exact nature, global distribution, and lifetime of these compounds is still far from being adequately elucidated. The presence of Fe-binding ligands is therefore omitted from the current model. Fe previously scavenged higher up in the water column is released back into solution if the host material is remineralized.

In the ocean interior the total change in the Fe inventory of each ocean cell (mol a^{-1}) can be written

$$\Delta M_{tot}^{Fe} = \Delta M_{ocn}^{Fe} + \Delta M_{remin}^{Fe} - \Delta M_{scav}^{Fe} \qquad (2\text{-}36)$$

where ΔM_{ocn}^{Fe} is the net change due to ocean advection, convective adjustments, and (horizontal and vertical) diffusivity, and ΔM_{remin}^{Fe} represents Fe both liberated from organic compounds through the remineralization of POM and from Fe scavenged by particulate matter further up in the water column and subsequently released through the remineralization of the scavenger substrate. ΔM_{remin}^{Fe} is defined

$$\begin{aligned}\Delta M_{remin}^{Fe} = {} & r^{POFe:POC} \cdot \left(Fset_{in}^{POC} - Fset_{out}^{POC} \right) + \\ & \frac{Fset_{in}^{POC} - Fset_{out}^{POC}}{Fset_{in}^{POC}} \cdot Fscav_{POC,in}^{Fe} + \\ & \frac{Fset_{in}^{opal} - Fset_{out}^{opal}}{Fset_{in}^{opal}} \cdot Fscav_{opal,in}^{Fe} + \\ & \frac{Fset_{in}^{cal} - Fset_{out}^{cal}}{Fset_{in}^{cal}} \cdot Fscav_{cal,in}^{Fe} + \\ & \frac{Fset_{in}^{arg} - Fset_{out}^{arg}}{Fset_{in}^{arg}} \cdot Fscav_{arg,in}^{Fe} \end{aligned} \qquad (2\text{-}37)$$

where $r^{POFe:POC}$ is the mean ratio of Fe:C in POM, and $Fset_{in}^{POC}$ and $Fset_{out}^{POC}$ out are the settling fluxes of POC into and out of the cell, respectively (mol a^{-1}). $Fscav_{POC,in}^{Fe}$ is the flux of scavenged Fe associated with POC into the cell, with the scavenged fluxes associated with opal ("opal"), calcite ("cal"), and aragonite ("arg"), similarly designated.

ΔM_{scav}^{Fe} is the loss (mol a^{-1}) of Fe due to scavenging by settling particulate matter

$$\begin{aligned}\Delta M_{scav}^{Fe} = {} & kscav_{POC}^{Fe} \cdot fset_{out}^{POC} \cdot M^{Fe} + \\ & kscav_{opal}^{Fe} \cdot fset_{out}^{opal} \cdot M^{Fe} + \\ & kscav_{cal}^{Fe} \cdot fset_{out}^{cal} \cdot M^{Fe} + \\ & kscav_{arg}^{Fe} \cdot fset_{out}^{arg} \cdot M^{Fe} \end{aligned} \qquad (2\text{-}38)$$

where $kscav_{POC}^{Fe}$ is the scavenging rate of Fe by POC (a^{-1} (mol m^{-2} a^{-1})$^{-1}$), with scavenging rates associated with opal ("opal"), calcite ("cal"), and aragonite ("arg"), similarly designated, and M the inventory of Fe within the cell (mol). $fset_{out}^{POM}$ is the particulate matter flux density out of the cell (mol m^{-2} a^{-1}) defined by

$$fset_{out}^{Fe} = \frac{Fset_{out}^{Fe}}{A} \qquad (2\text{-}39)$$

where A is the horizontal cross-sectional area of the cell (m^2).

For the surface ocean layer, the mass balance is

$$\Delta M_{tot}^{Fe} = \Delta M_{ocn}^{Fe} + \Delta M_{aeolian}^{Fe} - \Delta M_{scav}^{Fe} - \Delta M_{np}^{Fe} \qquad (2\text{-}40)$$

where $\Delta M_{aeolian}^{Fe}$ is the aeolian input of dissolved Fe from dust deposited to the surface, and ΔM_{np}^{Fe} is the loss of Fe due to biological uptake (and subsequent export)

$$\Delta M_{np}^{Fe} = r^{POFe:POC} \cdot Fnp^{POC} \qquad (2\text{-}41)$$

where Fnp^{POC} is the export flux of POC from the surface.

The aeolian input of dissolved Fe, $\Delta M_{aeolian}^{Fe}$ can be simply written

$$\Delta M_{aeolian}^{Fe} = \tfrac{1}{55.6} \cdot Fesol^{dust} \cdot Fefrac^{dust} \cdot Fdep^{dust} \qquad (2\text{-}42)$$

where $Fesol^{dust}$ is the mass fraction of aeolian Fe soluble in sea water, $Fefrac^{dust}$ is the mass fraction of Fe in aeolian dust, and $Fdep^{dust}$ is the deposition flux of dust to the surface ocean (g a^{-1}). The mean relative atomic mass of Fe, used to convert between mass and molar fluxes is taken to be 55.8 g mol^{-1}.

The mass fraction of Fe in aeolian dust ($Fefrac^{dust}$) can be reasonably assumed to be equal to the mean crustal abundance of 3.5% [*Duce and Tindale*, 1991]. However, estimating a representative global value for $Fesol^{dust}$ is much more problematic. Indeed, estimates reported for the solubility of aerosol Fe range over a full 3 orders of magnitude from <0.013 % to 55% [*Jickells and Spokes*, in press]. The most important controlling factor in determining overall solubility of Fe in sea water is likely to relate to the balance of aeolian material deposited between 'wet' and 'dry' deposition routes, as the solubility of Fe in rainwater (~14%) is considerably higher than that of Fe in seawater (0.1-1.0%) [*Jickells and Spokes*, in press]. However, the effective solubility of Fe in sea water via the 'wet' deposition route is reduced by the precipitation of insoluble iron

(hydr-)oxide phases associated with the *p*H change, to perhaps ~0.3-6.8% [*Jickells and Spokes*, in press; *Spokes and Jickells*, 1996]. Final solubility is also likely to be affected by the degree of remoteness of an oceanic region from dust source area, as the lability of iron in aerosols is enhanced through *p*H cycling within clouds [*Spokes and Jickells*, 1996]. Given these complications together with uncertainties regarding the balance between wet and dry dust deposition routes, $Fesol^{\text{dust}}$ is treated as an optimizable parameter, whose value(s) is chosen in order to be broadly consistent with the estimate of global mean solubility of *Jickells and Spokes* [in press] (0.8-2.1%).

A second important factor affecting overall aerosol iron solubility concerns the degree of system loading. For instance, *Zhuang et al.* [1990] showed that the soluble metal fraction decreased dramatically with increasing total iron content in seawater, while *Spokes and Jickells* [1996] found that solution concentrations were highly nonlinear with particulate loading. These effects may be related to (re-)adsorption of dissolved iron onto aerosol surfaces [*Chester et al.*, 1993]. A degree of 'self-scavenging' by aerosols in the ocean surface layer is therefore implemented in SUE. This implicitly produces an apparent Fe solubility which exhibits an inverse dependence on both [Fe] and dust flux, qualitatively consistent with observations. The surface ocean Fe mass balance (2-42) is now modified

$$\Delta M^{\text{Fe}}_{\text{aeolian}} = \tfrac{1}{55.6} \cdot Fesol^{\text{dust}} \cdot Fefrac^{\text{dust}} \cdot Fdep^{\text{dust}} - kscav^{\text{Fe}}_{\text{dust}} \cdot fdep^{\text{dust}} \cdot M^{\text{Fe}} \quad (2\text{-}43)$$

where $kscav^{\text{Fe}}_{\text{dust}}$ is a 'self-scavenging' rate constant (in units of a^{-1} $(g\ m^{-2}\ a^{-1})^{-1}$), and $fdep^{\text{dust}}$ is the dust deposition flux density ($g\ m^{-2}\ a^{-1}$) defined by

$$fdep^{\text{dust}} = \frac{Fdep^{\text{dust}}}{A} \quad (2\text{-}44)$$

Finally, aeolian iron not dissolved in the surface ocean is assumed to pass through the water column without further dissolution.

2.2.6 Carbon-13

As an aid to elucidating the function of the present-day global carbon cycle together with the causes of glacial-interglacial change, all major ^{13}C fractionation processes are represented within SUE. These relate to the dissolution equilibria within the aqueous carbonate system, biological fixation of both organic and inorganic carbon, and air-sea gas exchange.

In the subsequent sections, the following conventions will be adopted. From the ratio of the concentration of ^{13}C to ^{12}C in bulk matter

$$\mathrm{R(C)} = \frac{[^{13}\mathrm{C}]}{[^{12}\mathrm{C}]} \quad (2\text{-}45)$$

a fractionation factor is defined for any process, α where the chemical or physical state of carbon is transformed

$$\alpha(\mathrm{C} \rightarrow \mathrm{C}') = \frac{\mathrm{R(C)}}{\mathrm{R(C')}} \quad (2\text{-}46)$$

The fractionation associated with this process is more commonly written

$$\varepsilon = \alpha - 1 \quad (2\text{-}47)$$

where ε is quoted in units per mil (‰).

2.2.6.1 *Fractionation within the aqueous carbonate system*

The equilibrium partitioning of ^{13}C between the three primary reservoirs of the aqueous carbonate system is calculated explicitly (Figure 2-8). In this treatment, the net ^{13}C isotopic signature of $CO_{2(aq)}$ ($\delta^{13}C^{CO_{2(aq)}}$) is derived from bulk DIC ($\delta^{13}C^{DIC}$) by considering the fractionation with respect to both HCO_3^- and CO_3^{2-} and calculated in proportion to their relative aqueous concentrations [*Marchal et al.*, 1998b; *Yamanaka and Tajika*, 1996]. Although *Zhang et al.* [1995] suggested that the presence of ion complexes in seawater prevent this simple approach being valid, the error in this method is <0.2‰ under typical oceanic conditions. This scheme has the advantage over the use of a single empirical temperature-dependent function linking $\delta^{13}C^{CO_{2(aq)}}$ and $\delta^{13}C^{DIC}$ (e.g., *Mook et al.* [1974]) in that it is able to additionally account for the influence on $\delta^{13}C^{CO_{2(aq)}}$ of changes in ALK, DIC, and pressure (depth).

Equilibrium fractionation factors within the surface ocean carbonate system are adapted from *Zhang et al.* [1995], with fractionations α_1 and α_2 derived by correcting the observed fractionations $HCO_3^- \rightarrow CO_{2(g)}$ and $CO_3^{2-} \rightarrow CO_{2(g)}$, respectively, for the dissolution fractionation between $CO_{2(g)}$ and $CO_{2(aq)}$ (α_β). Writing in per mil notation, these become

$$\varepsilon_1 = -41.92 + 0.114 \cdot T \quad (2\text{-}48)$$

$$\varepsilon_2 = -24.07 + 0.057 \cdot T \quad (2\text{-}49)$$

where T is the ambient temperature (K). The fractionation between DIC and $CO_{2(aq)}$ can then be estimated from

$$\varepsilon_\Sigma = \frac{\varepsilon_1 \cdot [HCO_3^-] + \varepsilon_3 \cdot [CO_3^{2-}]}{[CO_2] + [HCO_3^-] + [CO_3^{2-}]} \quad (2\text{-}50)$$

2.2.6.2 *Fractionation during ocean-atmosphere gas exchange*

The one-way ocean→atmosphere and atmosphere→ocean fractionation factors, $\alpha_{o\rightarrow a}$ and $\alpha_{a\rightarrow o}$, respectively (Figure 2-8) are defined [*Siegenthaler and Munnich*, 1981]

$$\alpha_{o\rightarrow a} \equiv \alpha_\Sigma \cdot \alpha_k \quad (2\text{-}51)$$

$$\alpha_{a\rightarrow o} \equiv \alpha_\beta \cdot \alpha_k \quad (2\text{-}52)$$

where α_β is the equilibrium CO_2 solubility fractionation factor [*Zhang et al.*, 1995], equivalent to

$$\varepsilon_\beta = -2.65 + 0.005 \cdot T \qquad (2\text{-}53)$$

and α_k is the kinetic fractionation factor associated with CO_2 diffusion across the boundary layer. A value of -0.88‰ is assumed for ε_k, consistent with both the experimental measurements of *Zhang et al.* [1995] and theoretical calculation of *Siegenthaler and Munnich* [1981]. A (sea water) correction is made to $\varepsilon_{a\to o}$ [*Zhang et al.*, 1995], to give final descriptions for one-way ocean→atmosphere and atmosphere→ocean fractionation

$$\varepsilon_{o\to a} = \varepsilon_\Sigma - 0.88‰ \qquad (2\text{-}54)$$

$$\varepsilon_{a\to o} = \varepsilon_\beta - 1.08‰ \qquad (2\text{-}55)$$

2.2.6.3 *Fractionation during biological fixation of organic carbon*

The fractionation of ^{13}C during the formation of organic matter in the surface ocean is usually described by a fixed factor, typically assigned a value between -20 and -22‰ in global carbon cycle models [*Heinze*, 1994; *Maier-Reimer*, 1993; *Yamanaka and Tajika*, 1996]. However, the isotopic signature of organic constituents in marine plankton appears to vary strongly as a function of both latitude and SST [*Rau et al.*, 1989] against a background of relatively constant $\delta^{13}C^{DIC}$. Recent field and experimental observations suggests that the ambient concentration of $CO_{2(aq)}$ (itself a function of temperature) is a more important denominator [*Rau et al.*, 1992]. The isotopic composition of POC ($\delta^{13}C^{POC}$) is therefore parameterized with an explicit dependence on $[CO_{2(aq)}]$. The model of *Rea et al.* [1996] is adapted, assuming that the isotopic signature of exported POC reflects that of phytoplankton biomass. $\delta^{13}C^{POC}$ is therefore defined

$$\delta^{13}C^{POC} = \delta^{13}C^{CO_{2(aq)}} - \varepsilon_f + (\varepsilon_f - \varepsilon_d) \cdot \frac{Q_s}{c_e} \cdot \left(\frac{r}{D_T \cdot (1 + r / r_k)} + \frac{1}{P} \right) \qquad (2\text{-}56)$$

Where ε_f and ε_d are fractionation factors associated with enzymic intercellular C fixation and $CO_{2(aq)}$ diffusion, respectively, c_e is the ambient concentration of $CO_{2(aq)}$ (in units of mol m^{-3}), r is the surface area equivalent cell radius, r_k is the reacto-diffusive length, Q_s the $CO_{2(aq)}$ uptake rate per cell surface area, P is the cell wall permeability to $CO_{2(aq)}$, and D_T is the temperature-sensitive diffusivity of $CO_{2(aq)}$ in seawater given by

$$D_T = 5.019 \times 10^{-6} \cdot e^{\left(\frac{-E_d}{RT}\right)} \qquad (2\text{-}57)$$

where E_d is the activation energy of diffusion, R is the gas constant, and T the temperature (K). Parameter values are those used by *Rea et al.* [1996], with the exception of r and Q_s which follow *Rea et al.* [1997]. These parameters are summarized in Table 2-5.

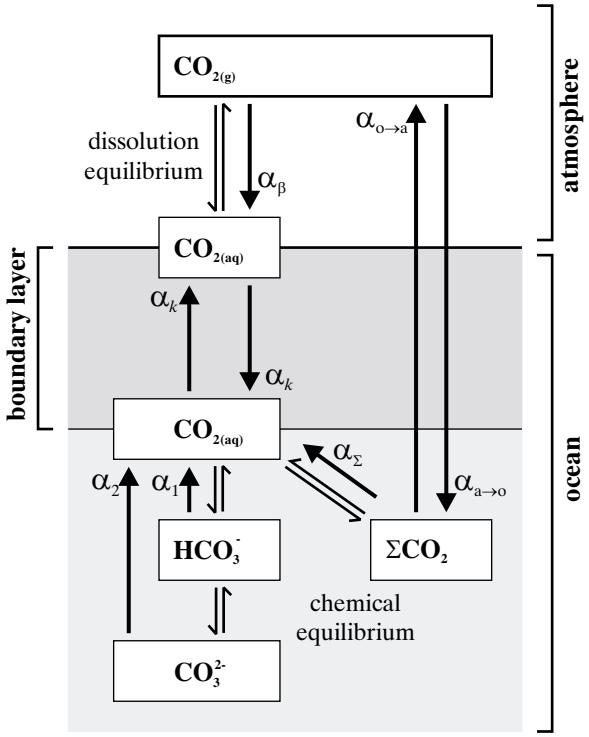

Figure 2-8 Schematic diagram of ocean-atmosphere ^{13}C and aqueous carbonate system fractionation, adapted from *Yamanaka and Tajika* [1996].

The description of $\delta^{13}C^{POC}$ (2-56) can be simplified

$$\delta^{13}C^{POC} = \delta^{13}C^{CO_{2(aq)}} - \varepsilon_f + (\varepsilon_f - \varepsilon_d) \cdot \frac{K_Q}{[CO_{2(aq)}]} \qquad (2\text{-}58)$$

where

$$K_Q = 1027 \cdot Q_s \cdot \left(\frac{r}{D_T \cdot (1 + r / r_k)} + \frac{1}{P} \right) \qquad (2\text{-}59)$$

and with $[CO_{2(aq)}]$ now in units of mol kg^{-1}. Finally, K_Q is approximated assuming that factors such as cell size are invariant

$$K_Q = 2.829 \times 10^{-10} - 1.788 \times 10^{-7} \cdot T + 3.170 \times 10^{-5} \cdot T^2 \qquad (2\text{-}60)$$

Despite the scheme of *Rau et al.* [1996,7] being able to successfully explain the main observational $\delta^{13}C^{POC}$ trend in the ocean, variations in $[CO_{2(aq)}]$ alone cannot account for the residual scatter and the more extreme outlying values [*Goericke and Fry*, 1994; *Rau et al.*, 1989, 1997]. Variability in vital factors such as cell size, growth rate, cell membrane

permeability, and diffusion rate will all affect the intercellular availability of $CO_{2(aq)}$ and thus overall fractionation [*Hinga et al.*, 1994]. Unfortunately, such parameters are not available in the simple biological model employed in SUE. However, since the biological scheme does differentiate between two distinct classes of phytoplankton (siliceous and non-siliceous) it is possible to represent species-specific factors, at least to a first order. While *Rau et al.* [1996, 1997] adopt an intermediate value of 25‰ for the enzymatic isotope fractionation factor associated with intracellular C fixation (ε_f), they note that it may actually range from 20 to 29‰. Indeed, *Hinga et al.* [1994] observed that $\delta^{13}C^{POC}$ in the diatom *Skeletonema costatum* was lower by some 8-10‰ compared to the coccolithophorid *Emiliania huxleyi* under identical growth conditions, possibly largely due to species differences in carbon fixation pathways [*Falkowski*, 1991]. Different values of ε_f associated with the two different classes of phytoplankton are therefore adopted, taking default values of 25‰ and 20‰, for siliceous and non-siliceous classes, respectively.

2.2.6.4 *Fractionation during the formation of calcium carbonate*

The formation of the carbonate tests of coccolithophorids and foraminifera and the shells of pteropods typically involves a degree of ^{13}C fractionation an order of magnitude less than that in the fixation of organic carbon. The 'carbonate pump' (2.1.1) therefore plays only a relatively minor role in determining spatial heterogeneity in $\delta^{13}C^{DIC}$ compared to action of the 'soft tissue pump'. However, since the permanent removal of carbon from the ocean is predominantly in the form of $CaCO_3$ [*Sarmiento and Sundquist*, 1992], $CaCO_3$ cycling is likely to be important in the long-term (glacial-interglacial) regulation of ^{13}C in the system. For this reason alone it is necessary to represent the fractionation $DIC \rightarrow CaCO_3$. To reproduce paleoceanographic foraminiferal $\delta^{13}C$ tracer signals observed in deep-sea sediments will also require a realistic treatment of the fractionation pathway $DIC \rightarrow CaCO_3^{foram}$.

Coccolith calcite and pteropod aragonite is assumed to make up bulk sedimentary $CaCO_3$. Simple temperature-dependent fractionation following *Mook* [1986] is assumed for this

$$\varepsilon_{HCO_{3(aq)}^{-} \rightarrow CaCO_3^{cal}} = \frac{4232.0}{T} + 15.10 \qquad (2\text{-}61a)$$

$$\varepsilon_{HCO_{3(aq)}^{-} \rightarrow CaCO_3^{arg}} = \frac{4232.0}{T} + 16.90 \qquad (2\text{-}61b)$$

In contrast, foraminiferal calcite is assumed not to contribute to the bulk sediment, but instead is treated as a tracer tied to bulk calcite (and as such does not contribute to mass transfer within the system). The simplest description of foraminiferal calcite $\delta^{13}C$ would be to assume an identical fractionation behaviour to bulk calcite. However, recent culture and modelling studies [*Spero et al.*, 1997; *Wolf-Gladrow et al.*, 1999a,b; *Zeebe et al.*, 1999] suggest that the concentration of carbonate ions ($[CO_3^{2-}]$) has an important controlling influence on fractionation. Empirically-determined relationships linking planktonic foraminiferal $\delta^{13}C$ to $[CO_3^{2-}]$ under conditions of constant DIC [*Spero et al.*, 1997] are therefore adopted (with reported shell $\delta^{13}C$ corrected for experimental $\delta^{13}C^{DIC}$). For the spinose *Orbulina universa*, $\delta^{13}C^{cal}$ is taken to be the mean of high light and dark responses (in a 50:50 proportion), while for the non-spinose *Globigerina bulloides*, $\delta^{13}C^{cal}$ is taken to be the mean of 12th and 13th chamber values [*Spero et al.*, 1997]. For *Orbulina universa* the resulting $DIC \rightarrow CaCO_3^{foram}$ fractionation can be written

$$\varepsilon_{\Sigma CO_2 \rightarrow CaCO_3^{foram}} = +1.795 - 0.006 \cdot [CO_3^{2-}] \text{‰} \qquad (2\text{-}62)$$

while for *Globigerina bulloides* it is

$$\varepsilon_{\Sigma CO_2 \rightarrow CaCO_3^{foram}} = -0.135 - 0.013 \cdot [CO_3^{2-}] \text{‰} \qquad (2\text{-}63)$$

where $[CO_3^{2-}]$ is the carbonate ion concentration in units of μmol kg^{-1}. As a default, *Globigerina bulloides* is assumed to represent the planktonic foraminiferal tracer in SUE. In the absence of comparable experimental data for benthic species the relationship for *Globigerina bulloides* is also used for the benthic foraminiferal tracer.

Table 2-5 Parameters Used in the ^{13}C POC Fractionation Model

Parameter	Value	Units
ε_f	20 to 29	‰
ε_d	0.7 [1]	‰
Q_s	1.62×10^{-7}	mol C m^{-2} s^{-1}
r	5.00×10^{-5}	m
E_d	19510	J mol^{-1}
R	8.3143	J K^{-1} mol^{-1}

[1] ε_d has a small temperature dependence in reality, but is assumed here to be constant.